LEGIBILITY NOTICE

A major purpose of the Technical Information Center is to provide the broadest dissemination possible of information contained in DOE's Research and Development Reports to business, industry, the academic community, and federal, state and local governments.

Although a small portion of this report is not reproducible, it is being made available to expedite the availability of information on the research discussed herein.

Los Alamos National Laboratory is operated by the University of California for the United States Department of Energy under contract W-7405-ENG-36

LA-UR--89-2127

DE89 014223

TITLE: THE HIGH-DENSITY Z-PINCH AS A PULSED FUSION NEUTRON SOURCE FOR FUSION NUCLEAR TECHNOLOGY AND MATERIALS TESTING

AUTHOR(S): R. A. Krakowski, J. D. Sethian, and R. L. Hagenson

SUBMITTED TO: International Energy Agency Workshop on Fusion Materials Irradiation Facilities, Bahia Hotel, San Diego, CA, February 14-17, 1989. Submitted to Journal of Fusion Energy

DISCLAIMER

Los Alamos National Laboratory
Los Alamos, New Mexico 87545

THE HIGH-DENSITY Z-PINCH AS A PULSED FUSION NEUTRON SOURCE FOR FUSION NUCLEAR TECHNOLOGY AND MATERIALS TESTING

R. A. Krakowski,* J. D. Sethian,† and R. L. Hagenson‡

ABSTRACT

The dense Z-pinch (DZP) is one of the earliest and simplest plasma heating and confinement schemes. Recent experimental advances based on plasma initiation from hair-like (10s μm in radius) solid hydrogen filaments have so far not encountered the usually devastating MHD instabilities that plagued early DZP experimenters. These encouraging results along with debut of a number of proof-of principle, high-current (1-2 MA in 10-100 ns) experiments have prompted consideration of the DZP as a pulsed source of DT fusion neutrons of sufficient strength ($\dot{S}_N \geq 10^{19}$ n/s) to provide uncollided neutron fluxes in excess of $I_\omega = 5\text{-}10\ MW/m^2$ over test volumes of 10-30 litre or greater. While this neutron source would be pulsed (100s ns pulse widths, 10-100 Hz pulse rate), giving flux time compressions in the range $10^5\text{-}10^6$, its simplicity, near-term feasibility, low cost, high-Q operation, and relevance to fusion systems that may provide a pulsed commercial end-product (e.g., inertial confinement or the DZP itself) together create the impetus for preliminary consideration as a neutron source for fusion nuclear technology and materials testings. The results of a preliminary parametric systems study (focusing primarily on physics issues), conceptual design, and cost *versus* performance analyses are presented. The DZP promises an inexpensive and efficient means to provide pulsed DT neutrons at an average rate in excess of 10^{19} n/s, with neutron currents $I_w \lesssim 10\ MW/m^2$ over volumes $V_{exp} \geq 30$ litre using single-pulse technologies that differ little from those being used in present-day experiments.

1. INTRODUCTION

Heating and confinement of high-density plasma by the self magnetic fields generated from plasma currents flowing between two electrodes is one of the earliest schemes considered in the quest for controlled thermonuclear fusion.[1] The formation and Ohmic heating of these high-density Z-pinches (DZPs) by fast-rising currents generally relied on a rapid implosion of a cylindrical current sheath onto the axis of the pinch. These early "classical" pinches were found to be highly unstable[1-3] to sausage ($m = 0$) and kink ($m = 1$)

* Los Alamos National Laboratory, Los Alamos, NM 87545

† Naval Research Laboratory, Washington, DC 20375-5000

‡ Phillips Petroleum Co., Bartlesville, OK 74004

magnetohydrodynamic (MHD) deformations. Linear, ideal (zero resistivity) MHD theory predicts[3-5] reduced growth rates, or even stability for the $m = 0$ mode, if the current profiles are sufficiently diffuse. Minimum pressure profiles for which the $m = 0$ mode is ideally and linearly stable have been reported.[4,5] The stabilizing effects of external gas pressure[4] or finite ion Larmor radius[6] have also been suggested.

The development of improved high-voltage, pulsed-diagnostic, and pinch-formation techniques together have led to improved results for the DZP[7] and an enhanced appreciation for the impact of formation conditions and plasma profiles on the pinch behavior. Recent DZP experiments at Los Alamos[8,9] and at the Naval Research Laboratory[10] have initiated high-voltage discharges through small-radius (10-40 μm), solid-deuterium fibers. These I = 0.3-0.6 MA experiments do not observe the $m = 1$ kink instability, and the $m = 0$ sausage instability is suppressed for 100s of Alfvén transit times across the pinch radius as long as the plasma current is increasing ($\dot{I} > 0$). While transport and stability analyses[11,12] are being conducted using three-dimensional resistive models in both linear and non-linear regimes, the stability of these fiber-initiated DZPs remains enigmatic, indicating the importance of formation method, pinch profiles, local (edge-plasma) dissipation, and dynamic stabilizing mechanisms. Activities organized to resolve these unknowns have recently been summarized.[13] Even more recently,[14] a Z-pinch workshop has summarized progress in this area.

These recent experimental and theoretical results warrant the examination of the potential and possible characteristics of the DZP as an intense source of DT neutrons for fusion nuclear technology testing[15,16] and other uses.[17] While a number of fusion reactor scoping studies of the DZP have been reported,[18-21] the potential of this approach as a small but intense source of fusion neutrons represents a more near-term application. A simplified analytic model[19,21] of the DZP has been used to examine parametric tradeoffs between plasma physics requirements, fusion neutron fluxes and currents, available test volume at a given neutron flux, and a range of operational characteristics. This early modeling effort assumed that the pinch current is increased in a way to assure a constant plasma radius and a balance between magnetic-field pressure and the plasma pressure; flat density and temperature profiles were assumed, alpha-particle heating and pressure was ignored, and the main device performance was characterized by either the number of Alfvén times, $N_A = \int_0^{\tau_D} dt/\tau_A$, across a pinch of radius a, ($\tau_A = a/v_A$ and v_A is the Alfvén speed) or the plasma current rise rate, $\dot{I}$. Under these idealized equilbrium conditon, when the Ohmic heating equals the Bremmsstrahlung losses, the pinch operates at the Pease-Braginskii current[22] of $I \simeq 1.5\text{-}2.0\ MA$, depending on temperature and density radial profiles. At a deeper level of analysis,[24] a connection must be made between pinch profiles, stability, and performance; this phase of the DZP neutron-source study is reported herein.

The projection of DZP performance as a pulsed neutron source remains largely in the modeling phase, and this summary report emphasizes this aspect of the problem. After briefly summarizing the essential elements of the DZP in the following Section 2, the plasma models used to estimate neutron yields, S_N, and efficiency, Q_P, are described and evaluated in Section 3 to yield a sample design point. These design-point results have yet to be translated into a conceptual engineering design, but these results are of

sufficiently detail to allow a preliminary economic and performance (e.g., test volume at a given neutron flux) evaluation to be made in Section 4. Preliminary conclusions are given in Section 5.

2. ESSENTIAL ELEMENTS OF THE DZP

Figure 1 depicts the DZP as a linear filament of plasma through which is passed an axial current of sufficient magnitude both to heat the pinch through Ohmic dissipation and to confine the resulting plasma pressure, $\sim 2\, nk_B T$, by the self magnetic fields associated with the axial plasma current. The combination of plasma heating and confinement in a linear geometry (10-30 μm radius $\times$ 0.05-0.10 m length) renders the DZP an elegance not enjoyed by most magnetically confined fusion systems. It is for this reason that the DZP was one of the earliest plasma-confinement schemes examined in the quest to control thermonuclear fusion.[1] The methods of forming these early pinches by means of fast implosion of current sheaths formed on the surface of the pinch gave rise to the two basic instabilities illustrated schematically on Figure 2. These instabilities along with impurity influx from the solid electrodes at each end of the pinch forced fusion research into directions that: (**a**) embedded axial magnetic fields for stabilization (of the m = 0 mode); and (**b**) eliminated the electrodes by forming the combined axial and encircling magnetic-field structure into a torus. Plasma stability and longevity was thereby achieved, but at the cost of simplicity and elegance.

Recent interest in the pulsed DZP has been centered on new ways to form a diffuse-current pinch (e.g., minimizing the radial sharpness of the current sheath) by applying a large voltage across a hair-like fiber of frozen deuterium (or DT in the case of the neutron source being considered here). The resulting pinch, which so far have passed 100s kA through a filament of 10s μm in radius, have shown surprisingly long stable times as long as the plasma current is rising ($\dot{I} \gtrsim 10^{12} A/s$). The time theoretically needed for this solid-fiber pinch to become unstable to the kinds of distortions depicted in Figure 2 is on the order of a/v_A; these modern DZPs have shown stability for $N_A \geq 100s$ of these Alfvén transit times, with values of $N_A \geq 1{,}000$ being the goal for the neutron source application.

The absence of the m = 0 instability can be explained by profile effects,[2] but the length of stable times for the m = 1 (kink) instability remains somewhat a puzzle and uncertainty for extrapolation of the DZP to high-Q fusion-burn conditions. Explanations for the observed stability include: (**a**) resistive effects, which explain the low-temperature m = 0 stability; (**b**) viscous effects, which explain the higher-temperature m = 0 stability; (**c**) skin effects, which are postulated to enhance the aforementioned effects of resistivity and viscosity; and (**d**) axial-flow effects to provide m = 1 stability at higher temperatures. The results of recent (and continuing) calculations by Nebel[12] on the impact of plasma resistivity on the m = 0, 1 instabilities are shown on Figure 3. Likewise, and in a more complex non-linear way, plasma viscosity can provide channels through which the energy that drives these instabilities can be dissipated; radial/axial coupling through Larmor gyrations, thermal flow along magnetic field lines, and compressional distortions of the pressure tensor provide dissipating mechanisms, each of which may be operative over different temperature regions.

Whatever the actual stabilization mechanisms active in the DZP, the experimentally observed stability in the modern DZP has been sufficiently reassuring to justify the construction of two major "proof-of-principle" experiments at the Naval Research Laboratory and at the Los Alamos National Laboratory. Table I summarizes the main parameters of each device, and Figure 4 gives a schematic diagram for each. The ZFX and HDZP-II experiments are complimentary, with the NRL device operating with a slower current rise rate (5×10^{12} A/s) and a somewhat higher-radius fiber (30-50 μm). At the heart of each device is a Marx-bank-driven fast energy store (a water capacitor for NRL, a water-filled transmission line for Los Alamos), and each has the planning and capability to use DT fibers. These devices, in size, energy, and cost, are prototypical of the DZP neutron source being proposed herein. In fact, the cost of constructing the Los Alamos HDZP-II experiment provides a realistic cost basis for estimating the DZP-based neutron source (Section 4). The technological challenges of operating this pulsed neutron source (10-100 Hz, 10-100 ns pulse width) are addressed qualitatively in Section 4, although considerably more work is required to resolve the technological issues related to 10-100 Hz pulse rates required of a $\dot{S}_N \geq 10^{19} n/s$ DZP neutron source.

3. DESIGN-POINT DETERMINATION

Preliminary scoping studies[16] of the DZP neutron source were made on the basis of a constant-radius analytic model that heated only by Ohmic dissipation, with Bremsstrahlung radiation being the only loss channel for plasma enthalpy. These early estimates[16] predicted that pinches of radius a $\simeq$15-20 μm and length $\ell_p \simeq$ 0.05-0.10 operating with discharge times $\tau_D \simeq$ 50 ns would produce a DT burnup fraction of $f_B = \simeq 0.05 - 0.10$ and a neutron yield of $S_N \simeq$0.5-1.0 $(10)^{17}$ ($W_F \simeq$ 0.1-0.2 MJ) with a Q-value of $Q_p \equiv W_F/W_B \simeq 1.0$, where $W_B \simeq \frac{1}{2} L_p I^2$ is the stored energy and L_p is the plasma inductance relative to the return conductor surrounding the pinch. These pinches typically would operate with a peak current of $I =$1.5-20 MA and require (for the value of τ_D given above) $V_p/\ell_p \simeq$5-10 MV/m from the Marx-charged water-filled transmission line; pulse rates in the range 10-100 Hz, therefore, would be required to give a neutron source strength $\dot{S}_N \simeq 10^{18}$-10^{19} n/s considered necessary for a high-flux ($I_w \gtrsim$ 5-10 MW/m^2), high-volume ($V_{exp} \simeq 10s$ of litres) neutron test facility.

While the analytic model of the DZP was adequate to determine the reasonableness of the concept, the compressional/expansional dynamics as well as fusion-product heating, burnup effects, enthalpy endloss, infusion of electrode impurities, plasma pressure and temperature profiles, and the waterline circuit can all impact the crucial parameters of the DZP neutron source, particularly S_N, Q_p, τ_D, and/or f_B. Consequently, the design-point determination was made using a coupled-plasma/circuits dynamical model described below. This modeling activity is continuing in considerably more detail[22,23] with the realization of the importance of a range of physical phenomena on the fusion burn dynamics and because of the eminency of single-discharge DZP experiments with parameters not significantly different from those suggested here for the neutron source.[13]

3.1 Model

The time-dependent, multi-species, profile-averaging (zero-dimensional), circuit-driven plasma model used to simulate reversed-field-pinch reactor plasmas[25] was modified to describe the DZP. A designated fraction of the energy associated with charged-particle fusion reaction products is deposited in the plasma, plasma enthalpy end losses are simulated as parallel electron conduction over regions of the plasma where the electrons are demagnetized, line-density depletion by fuel burnup is included, a range of plasma profiles consistent with the usual ($\nabla\vec{p} = \vec{j} \times \vec{B}$) equilibrium is included, and the radial transport of energy from the pinch other than radiation (line, cyclotron, and Bremsstrahlung radiations) is zero. Generally, axial energy transport by electron conduction is dependent on profile assumption, but is small, and the majority of the alpha-particle energy may be retained by the pinch.[26] A classical electrical resistivity was assumed with $Z_{eff} \simeq 1$, except as modified by alpha-particle accumulation. The complex process of fiber melting and plasma formation[27] was not modeled.

A range of plasma pressure/current profiles was examined in order to understand better the impact of possible stability constraints,[3,4,11,12] as well as the impact on the overall pinch dynamics and overall performance; these profiles were assumed to be frozen into the pinch, with more realistic multidimensional models[11] being required to examine diffusion effects. Two pressure profiles were considered that under widely differing assumptions could be stable to the $m = 0$ sausage instability: (a) the linearly ideally stable Kadomtsev profile;[4,5] and (b) a linearly non-ideally stable profile.[12] These extrema are respectively given by

$$p/p_0 = [5\beta/(4 + 5\beta)]^{\frac{5}{2}} \qquad (1A)$$

$$(4 + 5\beta)^{\frac{1}{2}}/\beta^{\frac{3}{2}} = \left[(5\beta_\theta - 1)^{\frac{1}{2}}/(\beta_\theta - 1)^{\frac{3}{2}}\right] x^2 \ , \qquad (1B)$$

and,

$$p/p_0 = 1 - 2x^\nu + x^{2\nu} \ , \qquad (2)$$

where $\beta = 2\mu_o p/B_\theta^2$ is the local beta, β_θ is $= 2\mu_o\langle p\rangle/B_\theta^2(1)$ is the average beta, and $x = r/a$ is the normalized pinch radius. Linear resistive stability is predicted[12] for the polynomial profile described by Eq. (2) when $\nu \geq 32$ (i.e., very flat radial pressure profile) for both $m = 0$ and $m = 1$ modes. The same model used to determine the stability of profiles given by Eq. (2) indicates that the Kadomtsev profiles are more than marginally stable if finite resistivity is included. Figure 6 gives the pressure and current density profiles for a range of assumed β_θ or ν values. The profile factors that correct the Bremsstrahlung, Ohmic, and DT-fusion powers computed using average properties, g_{BR}, g_{OHM}, and g_{DT}, respectively, with $g_{BR} = g_{DT}$ for a flat radial temperature profile, are also given on Figure 6.

A simplified algorithm was used to evaluate the waterline characteristics depicted on Figure 5 once the discharge time, τ_D, and the stored energy W_B, are specified. In addition to the plasma inductance

$$L_p = \frac{\mu_o l_p}{2\pi} \ln(R_o/a) \ , \qquad (3)$$

a range of "horizontal" and "vertical" gap inductances are computed, with the ratio f_L of stray to plasma inductances being computed that is consistent with the requirements of the main insulator stack (Figure 5) and magnetic insulation. Given the required field energy

$$W_B \simeq (1 + f_L)L_p I^2/2 \quad , \tag{4}$$

and a transfer efficiency, η_{WL}, the waterline capacitance can be computed from

$$C_{WL} = 2(W_B/\eta_{WL})/V_p^2 = \frac{2\eta\epsilon\ell_w}{\ell n(R_o/R_i)} \quad . \tag{5}$$

The length of the waterline is determined from the following expression for the discharge time:

$$\tau_D = 2\sqrt{L_{WL}C_{WL}} = \frac{2\ell w}{c}(\epsilon/\epsilon_o)^{1/2} \quad , \tag{6}$$

where c is the speed of light in vacuum, ϵ_o is the permittivity of free space, and ϵ is the the dielectric constant of water. From these expressions the ratio R_i/R_o can be computed. Finally, the following expression has been developed imperially by waterline designers[28] that relates the waterline standoff distance, $R_o - R_i$, to the applied voltage, V_p, the time of voltage standoff, τ_D, and the electrode area available for breakdown, $A_w \simeq 2\pi\ell w < R >$, where $< R >$ in the logarithmic average radius:

$$V_p\tau_D^{1/3}/10^6(R_o - R_i) \simeq 131.4/A_w^{0.08} \quad . \tag{7}$$

The results of a parametric evaluation of this waterline model are shown in Figure 7, where it has been assumed that $R_1 = R_i/2$ and $R_2 = (3/4)R_i$ (Figure 5). The electrical circuit is modeled as being composed of the coupled waterline/plasma elements depicted in Figure 8.

3.2 Results

As noted previously, the following processes that can impact device performance: (**a**) circuit efficiency (e.g., f_L *versus* τ_D, Figure 7); (**b**) plasma/circuit dynamics; (**c**) profile effects, particularly for Ohmic heating (Figure 6); (**d**) alpha-particle heating as contributing to expansion forces; and (**e**) axial energy transport. For each pressure profile, the temperature is assumed a constant of radius, and the impact of alpha-particle heating is examined parametrically. The discharge is assumed to terminate when $\dot{I} = 0$; the potential benefits of a crowbarred phase[19,24] in increasing f_B and Q_p are not taken into account. All computations fixed f_L at a conservative value of 0.5 while forcing τ_D and I, as well as the waterline geometry and W_{MX}, to adjust appropriately. Figure 9 and 10 give the time-dependent behavior of plasma temperature, density, radius, current, and powers for both the Kadomstev [Eq. (1)] and polynomial [Eq. (2)] pressure profiles, with and without alpha-particle heating; for both profiles, and for the plasma enthalpy endloss model used, alpha-particle self-heating can prematurely disrupt the pinch, causing premature expansion of the plasma column, a quenching of the burn, and a limitation on the Q-value and f_B. The dependence of Q_p and S_N, on N_A are shown in Figure 11 for

both the peaked (Kadomtsev) and polynomial ("poly") profiles, with and without alpha-particle heating; the results of the previously described analytic (constrained radius) model are also shown. Figure 12 shows the computed dependence of Q_p and S_N on peak plasma current; the strong dependence reported from experiment[10] is noted.

The general behavior with or without the inclusion of alpha-particle heating is similar between profiles for the fixed conditions assumed ($f_L = 0.5$, $a_o = 15\ \mu m$, $N = 3.88(10)^{19} m^{-1}$). For the Kadomtsev profiles, $g_{OHM} = 6.7$, $g_{BR} = g_{DT} = 6.5$, and $(g_{OHM}/g_{BR})^{\frac{1}{2}} = 1.02$, where the latter ratio is proportional to the equilibrium ($\dot{a} = 0$) Pease current, I_{eq}; these profile factors for the polynomial profiles ($\nu = 32$) are 3.76, 1.06, and 1.88, respectively. Hence, without alpha-particle heating, the stronger Ohmic heating early in the current transient gives a larger radial excursion for the Kadomtsev profile, but the final current is somewhat lower. The stronger internal fields for the Kadomtsev profile makes the axial end loss of energy by electron conduction negligible compared to 5% for the case of no alpha-particle heating in the case of the polynomial profile, and as high as 25-30% for the case of alpha-particle heating. For both profile cases considered, the initial plasma expansion, as driven by Ohmic heating, is turned around, and the plasma re-compresses to or beyond the original radius. It should be noted that the plasma/circuits dynamics in this early expansion phase is not well modelled by the zero-dimensional model.

Without alpha-particle heating, the assumed profiles set the time scale for the burn, with expected higher g_{OHM} and g_{DT} values for the Kadomtsev profile reducing that time scale somewhat. Generally, without alpha-particle heating, $T_e \simeq T_i$ for both profiles, but strong decoupling of T_e and T_i ($T_i > T_e$) is found with alpha-particle heating included for both profile cases. The impact of alpha-particle heating seems to be qualitatively the same for both profiles: to continue the radial expansion of the plasma column initially started by the Ohmic heating. Since g_{OHM} and g_{DT} are larger for the peaked Kadomtsev profile, the "blow up" of the pinch is more rapid, and the adverse impact on Q_P and S_N is greater (factor of $\sim$8 reduction for the Kadomtsev profile compared to 2.7 for the polynomial profile). The polynomial profile also benefits from an enhanced axial energy-loss rate to help shed the alpha-particle energy deposited into the plasma.

Combining all these effects, along with a greater separation of T_e and T_i when alpha-particle heating is included, gives the composite behavior summarized on Figures 11 and 12. On the basis of these simulations, a "strawman" design point has been selected using the polynomial pressure profile [Eq. (2), $\nu = 32$]. This design is summarized on Table II for the cases with and without alpha-particle heating. The latter $Q_p \simeq 1$ ($a_o = 15\ \mu m$, $\ell_p = R_c = 0.1\ m$) design ($S_N \simeq 2 \times 10^{17}\ n/pulse$, $\tau_D = 100\ ns$, $f_B \simeq 0.1$) is used to project the economics and general performance (I_w *versus* V_{exp}) of the DZP neutron source. However, it is emphasized that the burn dynamics of the DZP are complex, the present model uses only simplified models to described a limited number of physical processes and future work is required in this area to understand better important tradeoffs between physics, technology, performance, and cost.[24]

4. PRELIMINARY ECONOMICS AND PERFORMANCE EVALUATION

4.1 Cost Estimate

The DZP is a pulsed neutron source with significant time compression of the uncollided neutron flux. For example, the strawman design listed on Table II, with a 2×10^{17} $n/pulse$ source strength delivered in $\tau_D \simeq 100$ ns, would for an average source strength of $\dot{S}_N = 10^{19}$ n/s have to pulsed at a frequency of $\omega \simeq 50$ Hz, giving a flux compression of $FC \equiv 1/\omega\tau_D \simeq 2 \times 10^5$. Some leeway exists for reducing FC towards values where radiation damage rate effects are less of a concern to the material scientists, but the DZP can never approximate a truly steady-state source of neutrons. Reductions in FC generally reduce the per-pulse neutron yield (e.g., burnup fraction, f_B) and increase the repetition rate. While a few orders of magnitude reduction in FC are possible, the plasma Q-value decreases almost in proportion to f_B and, consequently, the cost of these more "steady-state-like" neutrons increases.

The positive side of this pulse nature is that these neutrons can be produced cheaply and fairly soon, give success of the DZP experiments presently coming on line at NRL (ZFX) and Los Alamos (HDZP-II). Since the DZP neutron source differs little from these experimental devices, with the exception of the pulse rate, and since significant costs are not anticipate in designing, building, and operating a 50-100 Hz DZP, cost projection for this pulsed neutron source as summarized in Table III, should be fairly accurate.

Table III gives only cost of the neutron source, *per se*. Before the generalized evaluation methodology described in Reference 29 can be applied to provide an overall, intercomparative figure-of-merit, the full capital cost of the DZP neutron facility must be estimated. The total capital cost is expected to exceed considerably the device cost summarized in Table III, but unfortunately the design of the overall facility has not available in sufficient detail to allow an accurate, "bottoms-up" cost estimate to be made. Consequently, an estimate of the total capital cost, CAP(M$), was made by scaling in size and power the more detailed estimates mode for the FTF/RFP.[29] Table IV summarize the results of this estimate, with CAP $\simeq$ 110 M$, after the cost of systems of no relevance to the DZP (e.g., coils current drive, etc.) was subtracted. As described in Reference 29, CAP is multiplied by a pay rate, $\lambda(\mathrm{yr}^{-1})$ and combined with other annual charges related to: (**a**) cost of people, COP (M$/person yr); (**b**) cost of electricity, COE (mills/kWeh); and cost of tritium, COT (M$/kg), to give the following expression for the total annual changes:

$$\mathrm{AC(M\$/yr)} = \lambda * CAP + N * COP + p_f P_F \left[\frac{COE}{114.2 * Q_p} + \frac{COT(1 - TBR)}{18.0} \right] . \qquad (8)$$

This annual charge is used in the following expression for a figure-of-merit, FOM, that reflects the cost of creating a given number of total lattice displacements with neutrons.

$$FOM(M\$/dpa \cdot m^3) = \frac{AC * T}{DPA * V_{exp}} . \qquad (9)$$

In these expressions, N is the number of people needed to operate the neutron source, p_f is the duty factor of the device, TBR is the tritium breeding ratio, $DPA/T \sim 10 I_w(MW/m^2)$

is the annual displacement rate, and $V_{exp}(m^3)$ is the experimental volume. Using the base-case values for these parameters listed in Table V, an annual charge of AC = 28 M$/year is estimated.

4.2 Performance Evaluation

In conducting a preliminary performance evaluation of the DZP neutron source, both the pulse-rate issues and the neutron flux distribution through the test volume must be resolved. Little detailed engineering has been devoted to the pulsed-rate issues, which center on: (a) power supply; (b) DT fiber injection; (c) electrode erosion; and (d) post-discharge evacuation of the discharge chamber.

Preliminary estimates of the plasma exhaust issue revealed no serious problem with evacuating the $\sim$ 1 litre-torr of unburn DT fuel, helium ash, and impurities on a $\lesssim 10^{-3}$s timescale for the geometry depicted in Figure 5 and summarized in Table II. Likewise, no serious operational on cost problems could be identified with the power supplies, with the main concern being the lifetime of the switches used in the Marx bank [re: footnote (a) in Table III].

A number of schemes for injecting the DT fiber into the discharge chamber on a $\sim$10 *ms* timescale have been considered, but none have been designed in sufficient detail to assure a good solution to this, along with electrode erosion, the greatest uncertainty with the DZP neutron course. Gravity feed of the frozen fibers would be adequate, continuous fiber extrusion with discharge "clipping" has been considered, or "blow-gun" injection using a gas-gun or electron-beam self-ablation drive are among the ideas being considered.

The problem of electrode longevity represents another serious issue for the DZP neutron source, both in terms impact on plasma performance and the economics and with respect to the essential feasibility of the 10-100 Hz DZP. Preliminary estimates[24] of impurity ingress into a $\ell_p \simeq 0.1$-m pinch from a lithium electrode indicates that, for discharges less than $\sim$300 *ns* in duration, the lithium evaporated at each electrode would have insufficient time to impact the burn dynamics and neutron yield. The main problem then revolves around resolving the geometry of a replenishable electrode. Lithium liquid metal seem particularly appropriate for this purpose, because of the relatively low melting point (459 K) and the low atomic number. Continuously extruded lithium rods or liquid-lithium jets are being considered. An example of the latter has been developed by NRL and is shown schematically in Figure 13.

As noted previously, any attempt to ameliorate the pulsed nature of the DZP neutron source will decrease f_B and therefore, Q_p; greater input power for a given source strength results. This point is illustrated schematically on Figure 14, which describes an idealized burn of duration τ_D that occurs with a period $1/\omega$ to yield a neutron-flux time compression of $FC = \dot{S}_N / < \dot{S}_N >_t = 1/\tau_D\omega$, where $\dot{S}_N$ is the neutron production rate averaged over the pulse width τ_D and $< \dot{S}_N >_t = \dot{S}_N \tau_D \omega$ is the time-averaged neutron production rate. Given that the time between pulses should be less than the time τ_V required for a lattice vacancy to recombine, a lower limit of $\omega \gtrsim 100$ Hz would be required for $\tau_V \simeq 10$ *ms*. An upper bound of $FC \lesssim 10^3$ then defines an operating space on Figure 14 that generally is not

achievable by the DZP in order to mimic a "steady-state" neutron source; burn times much above $\tau_D \simeq 100\ ns$ seem highly unlikely, particularly if the constrained that $\dot{I} \geq 10^{12}\ A/s$ must be enforced for reasons of stability. Hence, pulse frequencies in excess of 10 kHz would be required, and, given an average source strength of $< \dot{S}_N > \simeq 10^{19}\ n/s$, a burnup fraction of $f_B \leq 5 \times 10^{-4}$ would be required for the base-case conditions ($\ell_p = 0.1\ m$, $N \simeq 3.8 \times 10^{19}\ m^{-1}$) for $\omega = 10^4\ Hz$ (e.g., $2 < \dot{S}_N > /N\ell_p = f_B\omega$). The resulting Q-values for this system is given approximately by

$$\begin{aligned} Q_p = \frac{W_F}{W_{IN}} &= \frac{W_F}{\frac{1}{2}L_pI^2 + R_pI^2} \\ &= \frac{(E_F/T)f_B}{4\ell n(R_c/a) + 3(\tau_D/\tau_\Omega)} \\ &\simeq \frac{55\ f_B}{1 + \tau_D/10\tau_\Omega}\ , \end{aligned} \tag{10}$$

and would indeed be low for these low values of f_B; generally, the DZP cannot meet the steady-state criteria (e.g., $1/\omega < \tau_V$ and $FC < 10^3$) while simultaneously operating at $Q_p \gtrsim 1$ at moderate levels of neutron source strength ($< \dot{S}_N > \lesssim 10^{19}\ n/s$), even if kilocycle levels of pulse rates proved feasible.

While a number of ideas are available to deal with the main problems of the 10-100 Hz DZP neutron source, none have been developed to a level of integrated detail needed to assess the neutronic performance. Consequently, the idealized geometry shown in Figure 5 has been used to estimate the neutron flux and energy distribution. A two-dimensional Monte Carlo transport calculation was performed using the MCNP code.[30] The spacial distribution of 14-MeV neutrons and neutrons with energies above 0.18 MeV are shown in Figure 15 for this $\sim$ 50-Hz device; the MCNP computation modeled all vital parts of the DZP, including the topside cryogenic DT fiber maker, the bottomside alumna insulator stack, and the neutron-moderating water in the high-voltage transmission line. These preliminary estimates indicated severe heating problems in both the waterline insulators and the cryostatic fiber make for a 50-Hz, $\sim 10^{19}\ n/s$ device. Figure 16 gives the dependence of experimental volume on uncollided neutron flux for an $\dot{S}_N = 1.8 \times 10^{18}$ n/s device ($\sim$ 10 Hz). Combining the capital-cost estimate mode in Section 3.1 with the "standard" methodology described in Ref. 29, the resulting relative figure of merit for the DZP neutron source is shown in Figure 17. A comparison of this pulsed neutron source ($FC = 10^5$-10^6) with the steady-state RFP plasma-based neutron source is also given.

5. SUMMARY AND CONCLUSIONS

The DZP promises to fill a gap as a materials-testing facility of low-cost, moderate-to-high-flux fusion neutron source that can proivde DT neutron currents in the range $I_\omega =$ 5-10 MW/m^2 in 20-30 ℓ test volumes. This conclusion is based on an operating scenario where all fusions take place only during the current-rise phase, with a pinch termination assumed to occur when $\dot{I} \simeq 0$. The DZP is a strongly pulsed neutron source with neutron flux time compressions in the range 10^4-10^5; reductions in the flux compression is possible,

but the plasma Q-value would fall considerably below unity and the pulse rate would be in the kilo-Hertz range. By far the greatest physics uncertainty rests with attaining stable pinch times in the range N_A = 2,000–4,000, although it should be noted that for all cases the magnetic Reynold's number, $Re_m = \tau_\Omega/\tau_A$, is only in the range of 2,000-4,000. Initial liner melting, maintenance of pressure equilibrium, alpha-particle effects, the magnitude of plasma enthalpy endloss, and electrode impurity ingress present other important physics uncertainties requiring further study. Given that operation at high neutron fluxes proves possible by increases in the pulse rate substantially above ~1 Hz, minimizing the magnitude and cost of driver power, which is expected to be a main operational cost item, will require $Q_P \simeq 1$; this condition in turn translates into $N_A \gtrsim$ 4,000, with $f_B \gtrsim 0.05$ and $\dot{S}_N \tau_c \geq 0.8(10)^{17}$. As seen from Figure 11, these conditions and requirements can become easier or be made more difficult, depending on profile effects and whether or not the alpha particles couple energy/pressure to the pinch. Operation of the pinch beyond the $\dot{I}_\phi = 0$ cutoff enforced throughout this study will significantly increase the yield (burnup) and Q-value, although the MHD stability and technology required to "crowbar" the DZP represents an additional issue; it is nevertheless encouraging that the kinds of yields and fuel burnup (2-10% with alpha-particle heating, larger without alpha-particle heating) are theoretically possible during the current rise phase of 50-100 ns.

The main technical uncertainties are ones of energy transfer efficiency (as measured by $Q_p = W_F/W_{MX}$ and f_L), repetition rate, and damage rate effects [neutron flux time compressions in the range 10^5-10^6]. While the DZP is inherently a pulsed neutron source, not unlike those expected from inertial confinement fusion,[31-32] the pulse rate must be sufficiently high to allow operation at a thermal steady state with little or no (uncontrolled) temperature oscillation occurring in the test samples. Pulse rates of the order of $\gtrsim$ 1 Hz in this regard should be sufficient from an engineering viewpoint, except possibly for small-scale sample tests.

Related to this pulse-rate issue from an operational point of view is the ability to remove the unburned DT gas (~0.10 ℓ torr), the maximum injection rate of fresh DT fibers, and the pulsed-power requirements (1.5-2.0 MA at $V \simeq$ 2-5 MV). Other issues related to repetition rate are associated with switching of the Marx generators used to drive the high-voltage waterline, power reflections and dissipation therein, and electrode erosion and fatigue damage. High-repetition-rate Marx banks are available,[34] *albeit* at lower energies then required. Most of these pulse-rate technical issues appear amendable to reasonable technical solution within realistic cost and time constraints, although more detailed designs are required.

It should be emphasized that the physics of the DZP neutron source can be tested on a single-shot basis, without the need to develop critical technologies, on facilities presently coming into operation at NRL (ZFX) and Los Alamos (HDZP-II). If these experiments prove successful, the critical engineering components, (e.g., respectively, pulsed high-voltage power supplies, continuously pulsed fiber makers, a range of regenerative electrode configurations) can be developed in a "burst mode" on a prototypical device capable of discharging a short sequence of pulses. A typical development plan is suggested in Table VI based on this sequence of proof-of-principle (ZFX, HDZP-II) - burst-mode-

prototype→neutron-source-facility; the main components that would be tested and developed are indicated. A properly direct program of this kind should take approximately three years to provide a continuously operating 10^{18}-10^{19} n/s neutron source, given the physics of DZP stability allows the $\dot{I} > 0$ pinch to heat at nominally constant radius for 4,000-5,000 radial Alfvén times. The use of nominal existing and relatively uncomplex technology (no high-current accelerator, no high-power neutral beams, no high-field magnets, no high heat/particle-flux surfaces, etc.) promises a relatively inexpensive and rapid deployment of this pulse source of DT fusion neutrons.

In summary the DZP concept is emerging with new excitement generated by experimental sustainment times that go far beyond those predicted by MHD stability theories. Much of this progress can be attributed to a greater appreciation of the role played by the early formation and internal structure of the pinch, although much remains to be understood in this area.[27] The focus of ongoing efforts will be on understanding the implications of these formation and structural aspects of the DZP, as well as the impact of the driver circuit, in so far as they determine the operation of a high-Q, transitory ($\dot{I} \simeq 0$) source of fusion neutrons.

REFERENCES

1. O. A. Anderson, W. R. Baker, S. A. Colgate, J. Ise, Jr., and R. V. Pyle, "Neutron Production in Linear Deuterium Pinches," *Phys. Rev.* **110**(6), 1375 (1968).

2. J. Shiloh, A. Fisher, and E. Bar-Avraham, "Interferometry of a Gas-puff Z-pinch Plasma," *Appl. Phys. Lett.* **35**(5), 390 (1979).

3. N. R. Pereira, N. Rostoker, and J. S. Pearlman, "Z-Pinch Instability with Distributed Current," *J. Appl. Phys.* **55**(3), 704 (1984).

4. B. Kadomtsev, "Hydromagnetic Stability of a Plasma," *Rev. of Plas. Phys.* **2**, 153 (1966).

5. B. R. Suydam, "Effect of the Gas Blanket on the Stability of the Dense Z-Pinch," Los Alamos National Laboratory report LA-7809-MS (1979).

6. W. Hartman, "Finite Larmor Radius Stabilized Z-Pinches," Lawrence Livermore National Laboratory report UCID-17118 (1976).

7. M. G. Haines, *Phil. Trans. Roy. Soc. Lond.* **300A**, 649 (1981).

8. D. W. Scudder, "Experiments on High-Density Z Pinches Formed form Solid Deuterium Fibers," *Bull. Am. Phys. Soc.* **30**, 1408 (1985).

9. D. W. Scudder, R. Y. Dagazian, J. E. Hammel, P. R. Forman, "Solid Deuterium Fiber Z Pinches: Experiment and Theory," *Bull. Am. Phys. Soc.* **31**, 1581 (1986).

10. J. D. Sethian, A. E. Robson, K. A. Gerber, A. W. DeSilva, "Enhanced Stability and Neutron Production in a Dense Z-Pinch Plasma Formed form a Frozen Deuterium Fiber," *Phys. Rev. Lett.* **59**(8), 892 (1987).

11. R. A. Nebel, H. R. Lewis, J. E. Hammel, D. W. Scudder, P. Rosenau, "1-D Transport Calculations for Z-Pinch Fibers," to be published (1989).

12. R. A. Nebel, J. R. Lewis, I. R. Lindemuth, R. A. Nebel, P. Rosenau, "Multidimensional MHD Simulations of Dense Z-Pinch Fibers," *Bull. Am. Phys. Soc.* **32**(9), 1758 (1987).

13. A. H. Glasser, "Z-Pinch and Plasma Focus: Report on the 1988 Workshop on Z-Pinch and Plasma Focus," Nice, France (October 10-11, 1988), *Nucl. Fus.* **29**, 129 (1989).

14. Proc. 2nd Conf. on Dense Z-Pinches, April 26-28, 1989, Laguna Beach, CA.

15. M. A. Abdou, "Modeling, Analysis, and Experiment for Fusion Nuclear Technology," University of California at Los Angeles report PPG-1021 (January 1987).

16. R. Hagenson, J. Hammel, R. Krakowski, R. Miller, R. Nebel, D. Scudder, and K. Werley, "The High-Density Z-Pinch (HDZP) as a Fusion Neutron Source," Proc. 12th IEEE Symposium on Fusion Engineering **2**, 835 (1987).

17. R. W. Moir and R. S. Frost (eds.) "Study of a Magnetic Fusion Production Reactor" Lawrence Livermore National Laboratory report UCRL 94408 (1980).

18. C. W. Hartman, G. Carlson, M. Hoffman, R. Werner, and D. Y. Cheng, "A Conceptual Fusion Reactor Based on the High-Plasma-Density Z-Pinch," *Nucl. Fus.* **17**(5), 909 (1977).

19. R. L. Hagenson, A. S. Tai, R. A. Krakowski, and R. W. Moses, "The Dense Z-Pinch (DZP) as a Fusion Power Plant: Preliminary Scaling Calculations and Systems Energy Balance," *Nucl. Fusion* **21**(11), 1351 (1981).

20. M. G. Haines and S. P. Walker, "Compact Fusion Reactors: The Potential of the Dense Z-Pinch," *Nucl. Energy* (1987).

21. R. L. Hagenson, A. S. Tai, R. A. Krakowski, and R. W. Moses, "The Dense Z-Pinch (DZP) as a Fusion Power Reactor: Preliminary Scaling Calculations and Systems Energy Balance," Los Alamos Scientific Laboratory report LA-8186-MS (1980).

22. R. S. Pease, "Equilibrium Characteristics of a Pinched Gas Discharge Cooled by Bremsstrahlung Radiation," *Proc. Phys. Soc.* **70B**, 11 (1957).

23. S. Glasstone and R. H. Loveberg, "Controlled Thermonuclear Reactions," p. 226, Van Nostrand Reinhold Co., NY (1960).

24. R. A. Krakowski, "Fusion Burn Dynamics in Dense Z-Pinch (DZD)," Los Alamos National Laboratory report, to be published (1989).

25. R. L. Hagenson, et al., "Compact Reversed-Field Pinch Reactors (CRF R): Preliminary Engineering Consideration," Los Alamos National Laboratory report LA-10200-MS (1984).

26. R. H. Loveberg, "Retention of DT Alpha Particles in the Density Z-Pinch," personal communication, Los Alamos National Laboratory (April, 1989).

27. I. R. Lindemuth, G. H. McCall, and R. A. Nebel, "Fiber Ablation in the Solid-Deuterium Z Pinch," *Phys. Rev. Lett.* **62**(3), 264 (1989).

28. J. C. Martin and I. D. Smith, "Pulsed-Power Notes,' Atomic Weapons Research Estab., Aldermaston, UK (1965).

29. C. G. Bathke R. A. Krakowski, R. L. Miller, K. A. Werley," The Reversed-Field-Pinch (RFP) Fusion Neutron Source: a Conceptual Design," International Energy Agency workshop on Fusion Materials Irradiation Facilities, Bahia Hotel, San Diego, CA, February 14-17, 1989 (this proceedings).

30. Los Alamos Monte Carlo Group, "MCNP - A General Monte Carlo Code for Neutron and Photon Transport," Los Alamos National Laboratory report LA-6396-MS, revised (April, 1981).

31. N. M. Ghoniem and G. L. Kulcinski, "A Critical Assessment of the Effects of Pulsed Irradiation on the Microstructure Swelling, and Creep of Materials," *Nucl. Tech. Fus.* **2**(2), 165 (1980).

32. E. P. Simonen, N. M. Ghoniem, and N. H. Packan, "Pulsed Flux Effects on Radiation Damage," *J. Nucl. Mat.* **122** and **123**, 391 (1984).

33. G. L. Kulcinski and M. E. Sawan, "Differences between Neutron Damage in Inertial and Magnetic Confinement Fusion Test Facilities," *J. Nucl. Mat.* **133** and **134**, 52 (1985).

34. J. Shannon, 2nd IEEE Int. Pulsed Power Conf., Lubbock, TX, p. 226 (June 12-14, 1979).

FIGURE CAPTIONS

Figure 1. Schematic representation of the dense Z-pinch (DZP)

Figure 2. Schematic representative of the m = 0 ("sausage") and m = 1 ("kink") instabilities that commonly plagued the DZP.

Figure 3. The impact of plasma resistivity on the m = 0,1 instabilities (Figure 2) in the DZP.

Figure 4. Schematic diagrams of proof-of-principle DZP experiments under construction at the Naval Research Laboratory (ZFX) and the Los Alamos National Laboratory (HDZP-II).

Figure 5. Conceptual arrangement of the DZP neutron source showing schematically the Marx generator, water-filled transmission line, insulator stack, pinch chamber, DT fiber maker, and test volume. This model also provides a geometry for the first estimates of neutron fluxes, and dimensions show are used for estimating waterline design.

Figure 6. Pressure and current-density profiles and profile factors for two (extreme) test cases [Eq. (1) and (2)] examined by parametric design study.

Figure 7. Interdependence of waterline characteristics as a function of discharge time using the geometric described on Figure 5 and Eqs. (3)-(7).

Figure 8. Plasma/waterline circuits model used in time-dependent DZP simulation.

Figure 9. Commuted DT discharge for the Kadomstev profiles [Eq. (1)] with and without alpha-particle heating.

Figure 10. Computed DT discharges for the polynomial profiles [Eq. (2)], with and without alpha-particle heating.

Figure 11. Dependence of neutron yield and plasma Q-value on number of Alfvén times, N_A, for a range of pressure profiles, including the flat profiles assumed for the constant-radius analytic model. All discharges were terminated when $\dot{I} < 0$, and the impact of alpha-particle heating is shown (Figures 9-10).

Figure 12. Dependence of neutron yield and plasma Q-value on peak plasma current.

Figure 13. A liquid-lithium electrode concept being considered as a means to provide replenishable electrodes to the 10-100 Hz DZP.

Figure 14. Illustrations of pulse-rate and flux-compression limitation for the DZP neutron source.

Figure 15. High-energy and low-energy neutron flex distributed for a 50-Hz, $S_N \sim 10^{18}$ n/s DZP neutron source based on the geometry given in Figure 5.

Figure 16. Dependence of experimental volume on uncollided neutron current for the DZP geometry depicted in Figure 5.

Figure 17. Dependence of relative figure of merit on available test volume and comparison with the RFP neutron source.

TABLE I

Parameters for Proof of Principle DZP Experiments under Construction of the Navel Research Laboratory (ZFX) and the Los Alamos National Laboratory (HDZP-II).[a]

	Naval Research Laboratory (ZFX)	Los Alamos National Laboratory (HDZP-II)
Pinch length, $\ell_p(m)$	0.05	0.05
Pinch current, $I(MA)$	2.0	1.4
Waveform	Sinusoidal	Quasi-sinusoidal
Quarter-period, $\tau_D(ns)$	630	>100
Initial dI/dt, $(10^{12}A/s)$	5	25
Voltage, $V_p(MV)$	0.75	3.0
System energy, $W_B(kJ)$	350	200

(a) Both facilities are expected to be operational in 1989.

TABLE II
"Strawman" Resign Parameters for a DZP Neutron Source for for Use in Economic and Performance Evaluation.

	With α s	Without α s
Profile factors, g_i		
• $g_{BR} = g_{DT}$	1.057	1.057
• g_{OHM}	3.758	1.378
Aipha-particle heating, f_α	1	0
Current rise time, $\tau_R(ns)$	96.4	96.1
Voltage, $V_{WL} = V_{MX}$ (MV)	10.1	10.1
Stored Energy, W_{MX} (kJ)	537.	537.
Water-line efficiency, η_{WL}	0.98	0.98
Transfer efficiency, f_L	0.5	0.5
Plasma current, I_ϕ (MA)	1.86	1.81
Neutron yield		
• Energy, W_N (kJ)	157.7	421.2
• Number, $S_N/10^{17}$	0.70	1.87
Plasma Q-value, $Q_P = W_F/W_{MX}$	0.37	0.98
Number of Alfvén times, N_A	2990	4200
Plasma energies (kJ)		
• Ohmic, W_{OHM}	27.6	41.5
• Alpha particle, W_α	39.4	105.8
• Axial conduction, W_{COND}	11.6	7.83
• Radiation		
- Bremsstrahlung, W_{BR}	6.6	13.9
- Line (oxygen), W_{LINE}	nil	nil
- Cyclotron, W_{CYC}	nil	nil
• Expansion, W_{PV}	21.9	-6.1
• Plasma, W_p	27.6	26.2
Fuel burnup, f_B	0.036	0.095
Final Z_{eff}	1.04	1.10
Final plasma parameter		
• Line density, $N = \pi a^2 n\ (10^{19}/m)$	3.88	3.88
• Density, $n_i(10^{28}/m^3)$	0.38	3.07
• Temperature, T_e/T_i (keV)	10.1/20.1	14.9/14.7
• Expansion, $x = a/a_0$	3.68	1.47

TABLE II
"Strawman" resign parameters for a DZP neutron source for for use in economic and performance evaluation. (Cont.-1)

Geometry	
• Initial plasma radius, $a_o(\mu m)$	15
• Plasma length, $\ell_p(m)$	0.10
• Return conductor radius, $R_p(m)$	0.10
• Front end[a]	
– magnetically insulated gap, $\delta_g(m)$	0.01
– insulator-stack height, $\ell_i(m)$	0.83
– insulator-stack radii, $R_1/R_2(m)$	0.24/0.35
– inductances (pH)	
- · insulator, L_i	67.9
- · gap 1, L_{g1}	19.4
· - gap 2, L_{g2}	0.08
- · plasma, L_p	175.9
• Waterline	
·· length, $\ell_{WL}(m)$	1.44
– inner/outer radii, $R_i/R_o(m)$	0.47/0.86
– inductance, $L_{WL}(\mu H)$	0.17
·· capacitance, $C_{WL}(pF)$	10.63
• Marx bank	
·· inductance, $L_{MX}(\mu H)$	17.4
– capacitance, $C_{MX}(pF)$	10.1
– voltage, $V_{MX}(MV)$	10.1
– energy, $W_{MX}(kJ)$	537.0

(a) Refer to Figure 5.

TABLE III

Preliminary Cost Estimate of the DZP Neutron Source (Basic Revise Only) Based on the Cost to Build the Los Alamos HDZP-II Device.

	HDZP-II			DZP n-Source	
	Item	Cost (k$)	Unit Cost	Item	Cost (k$)
Pulse Rate (Hz)	~0			10	
Marx Bank[a]		100	0.5 $/kg		270
• Energy (kJ)	200			540	
• Dimensions (m)	$1.5 \times 3.0 \times 1.5 = 6.8\ m^3$			$18\ m^3$	
• Energy Density (kJ/m^3)	29			30	
Transmission Line[b]		100	167 $/kg		500
• Mass (tonne)	0.6				
• Dimensions (m, $\ell \times r_i/r_o$)	$1.83 \times 0.57/0.79$			$1.44 \times 0.47/0.86$	
Load Chamber[c]		50			100
• Dimensions (m, $\ell \times r$)	0.3×0.15			0.1×0.1	
• Volume (ℓ)	42			3.1	
Fibermaker[d]		2			50
Power Supply		20	1 $/W		5,400
• current (A)	0.2				
• voltage (kV)	100				
• power (kW)	20			5,400	
Tank[e]		55	3.7 $/kg		150
• mass (tonne)	15			41	
• dimensions (m)	$3.4 \times 3.1 \times 8.5 = 9.0\ m^3$			$24\ m^3$	
• nominal densities					
- energy (kJ/m^3)	2.2			22.5	
- mass ($tonne/m^3$)	1.7			1.7	
Vacuum		1			50
• speed (ℓ/s)	300			300	
TOTAL COST (k$)		328			6,520

(*a*) For both the HDZP-II experiment and the DZP n-source, approximately 0.1 Coulomb is discharged through a given switch, which for a lifetime charge transfer of 10^6 Coulomb amounts to $\sim 10^7$ discharges or switch lifetime of ~4% (~2 weeks) of a year for 80% availability. Replacement of those (~$100) items is expected to have a negligible impact on operating cost or availability.

(*b*) Although the high-voltage transmission lines for both the HDZP-II and the DZP n-source are nominally of the same dimensions, the n-source application would be more highly stressed and an arbitrary factor of 5 has been included in costing this item.

(*c*) A factor of two has been included in the nevertheless smaller load chamber required of the n-source to account for the added cost of accommodating irradiation samples and active cooling.

(*d*) This cost for the n-source taken arbitrarily 25 times that of the HDZP-II experiment to accommodate the impact of 10-Hz operation on this yet-to-be-designed item.

(*e*) The tank mass for the n-source was estimated from the HDZP-II "smear" density using a volume that accommodates the increased requirements of the higher-energy Marx bank, itself operated at the effective HDZP-II energy density, while allowing the nominal added ~ $8\ m^3$ for the HDZP-II-like transmission line.

TABLE IV
Preliminary Total Cost Estimate Scaled From Detailed Estimate made for FTF/RFP[30]

ITEM	(M$)
Front-end Device Cost	7.0[(a)]
Power	
• Supply	5.0
• Distribution	3.0
Diagnostics	7.0
Maintenance services	25.0
Data acquisition, control, processing	4.0
Watercooling/heat rejection	2.0
Tritium fueling system	1.0
Buildings, facilities, utilities	46.0
Cleanup, disposal, monitoring	2.0
Project cost	8.0[(b)]
Total	110.

(*a*) Taken from Table III

(*b*) 8% of total of above items.

TABLE V
Typical Parameters Used to Evaluate the Figure of Merit (FOM) for the DZP Neutron Source

Annual cost of money, λ (1/yr)	0.15
Number of people required to operate device, N	25.
Cost of people, $COP(M\$/person\ yr)$	0.16
Availability, p_f	0.8
Cost of electricity, $COE(mills/kWeh)$	40.
Cost of tritium, $COT(M\$/kg)$	10.
Tritium breeding ratio, TBR	0.0
Tritium burn-up fraction, f_B	0.05
dpa goal value, DPA	100.
Irradiation time to achieve DPA, $T(yr)$	1.0
Normalized dpa rate, $DPA/I_w T(dpa\,m^2/MW/yr)$	10.

TABLE VI
Typical Development Scenario for the DZP Neutron Source

Phase / Component	Proof of principle	Prototype (burst)	Facility
	Test physics (single shot)	Develop critical technologies (100 Hz for 1 s)	(100-Hz, continuous)
Power supply	Marx/waterline	DOD technology-burst	Continuous
Fibermaker	Manual extrusion	Pellet inject-burst	Continuous
Electrodes	Metal	Rotating solid	Lithium streams
Pumping	Turbo/diffusion	Large reservoir	Large pumps
Heat transfer	NA	Thermal capacity	Existing technology
Tritium handling	0.5 Curie/shot	50 Curie/burst	Fusion technology
Development time	< 2 years	3 years	3 years

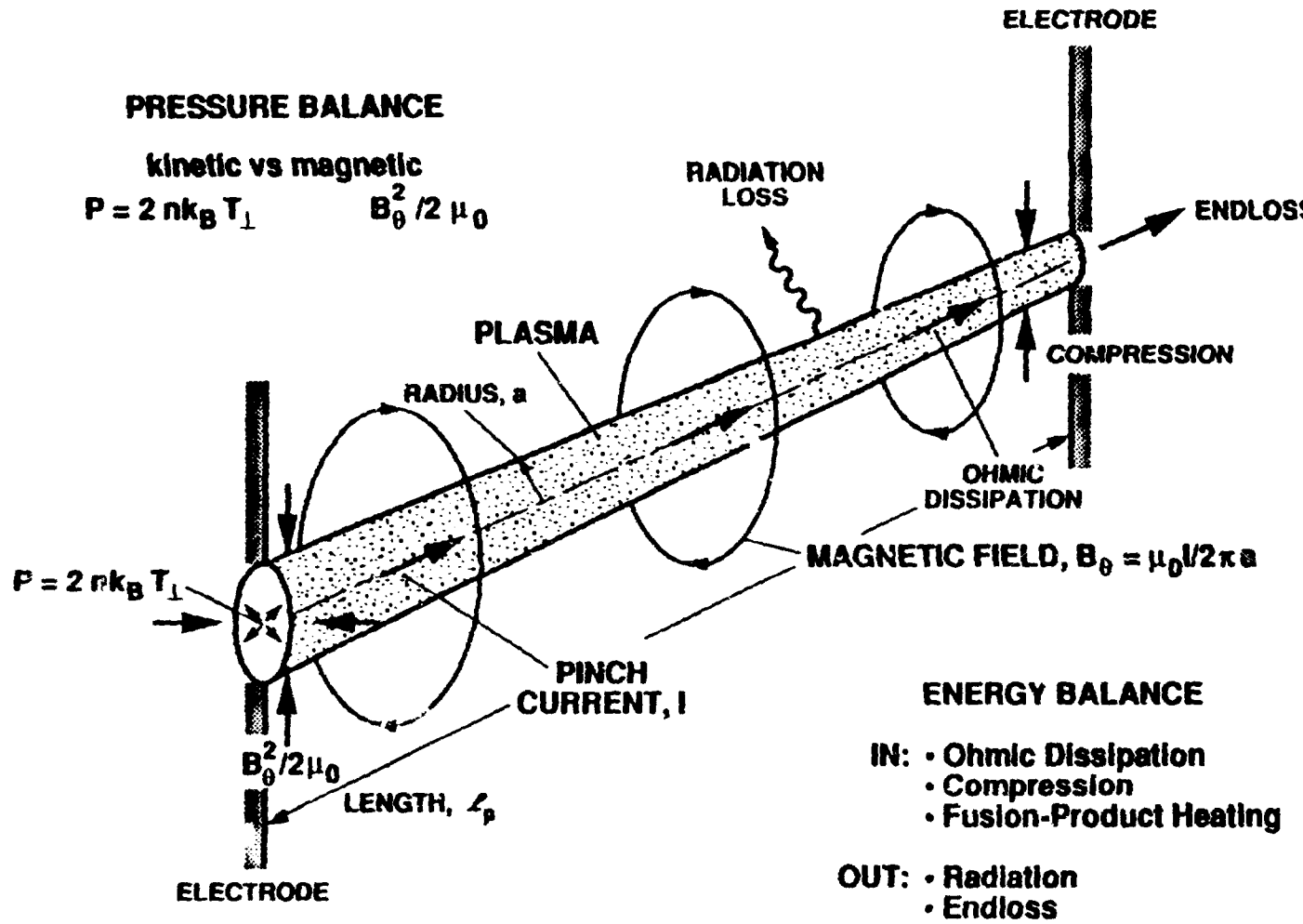

ENERGY BALANCE

IN:
- Ohmic Dissipation
- Compression
- Fusion-Product Heating

OUT:
- Radiation
- Endloss

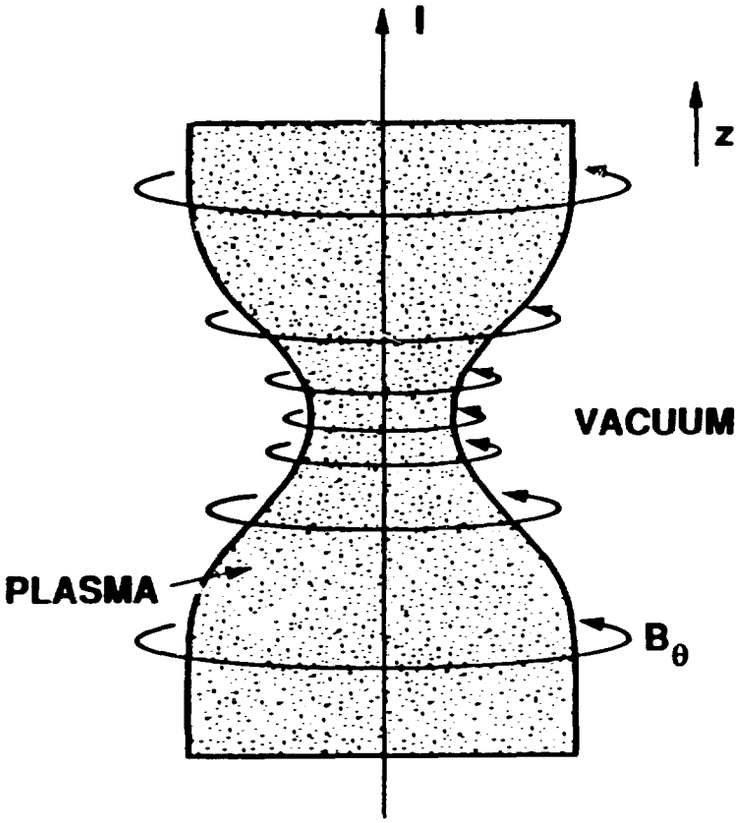

"SAUSAGE" (m = 0)
INSTABILITY

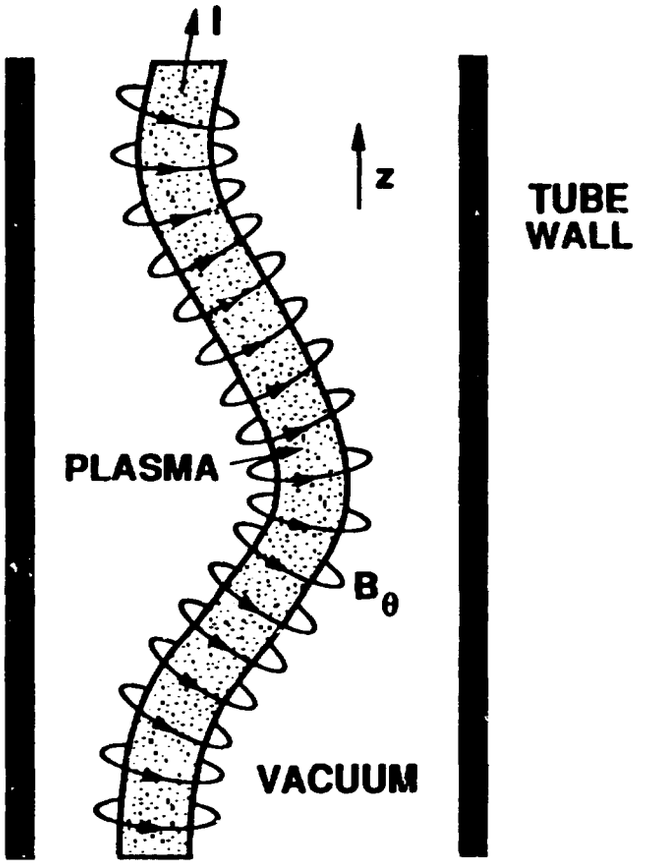

"KINK" (m = 1)
INSTABILITY

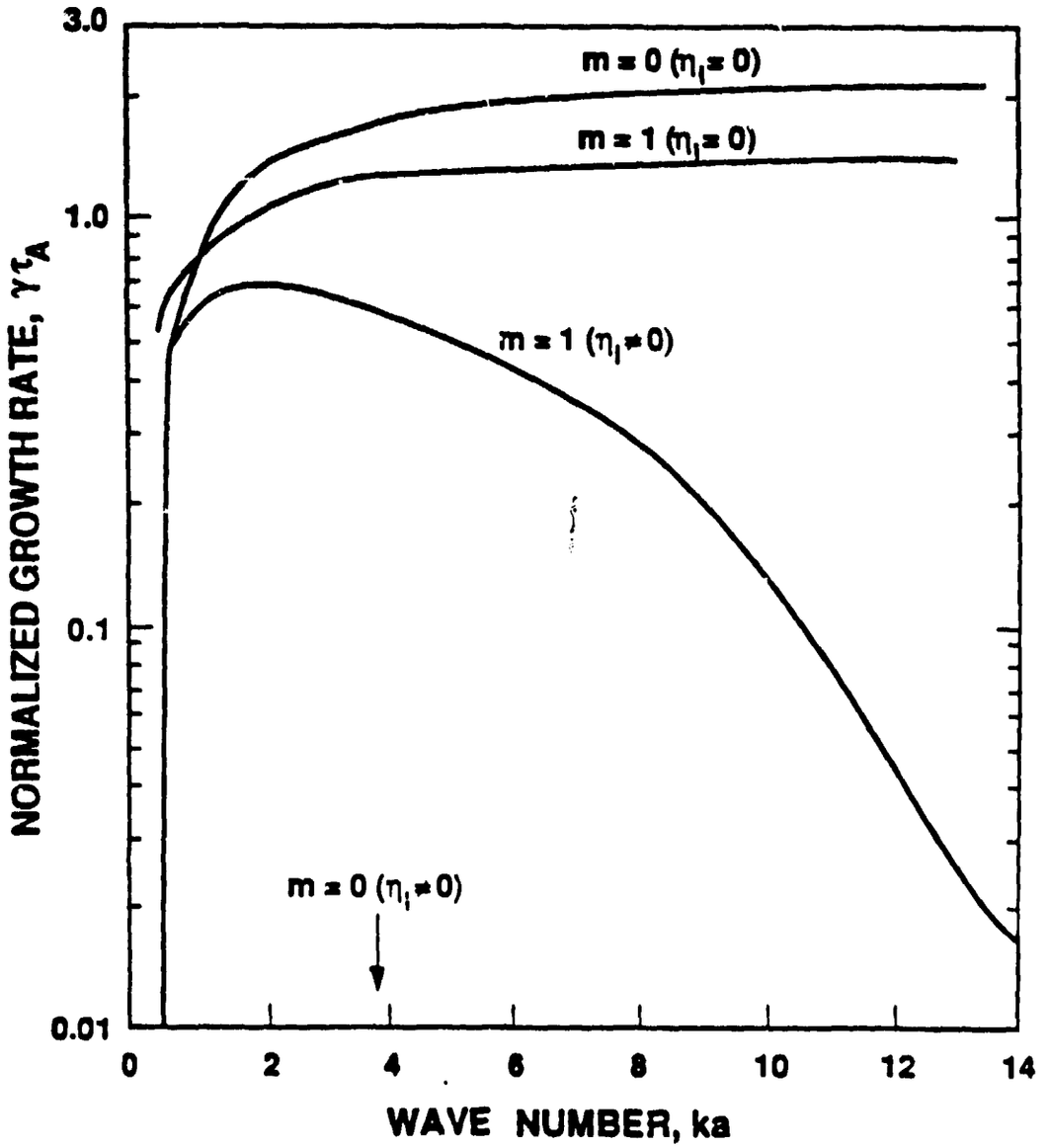
3.0
1.0
0.1
0.01
NORMALIZED GROWTH RATE, $\gamma\tau_A$
m = 0 (η_i = 0)
m = 1 (η_i = 0)
m = 1 ($\eta_i \neq 0$)
m = 0 ($\eta_i \neq 0$)
0
2
4
6
8
10
12
14
WAVE NUMBER, ka

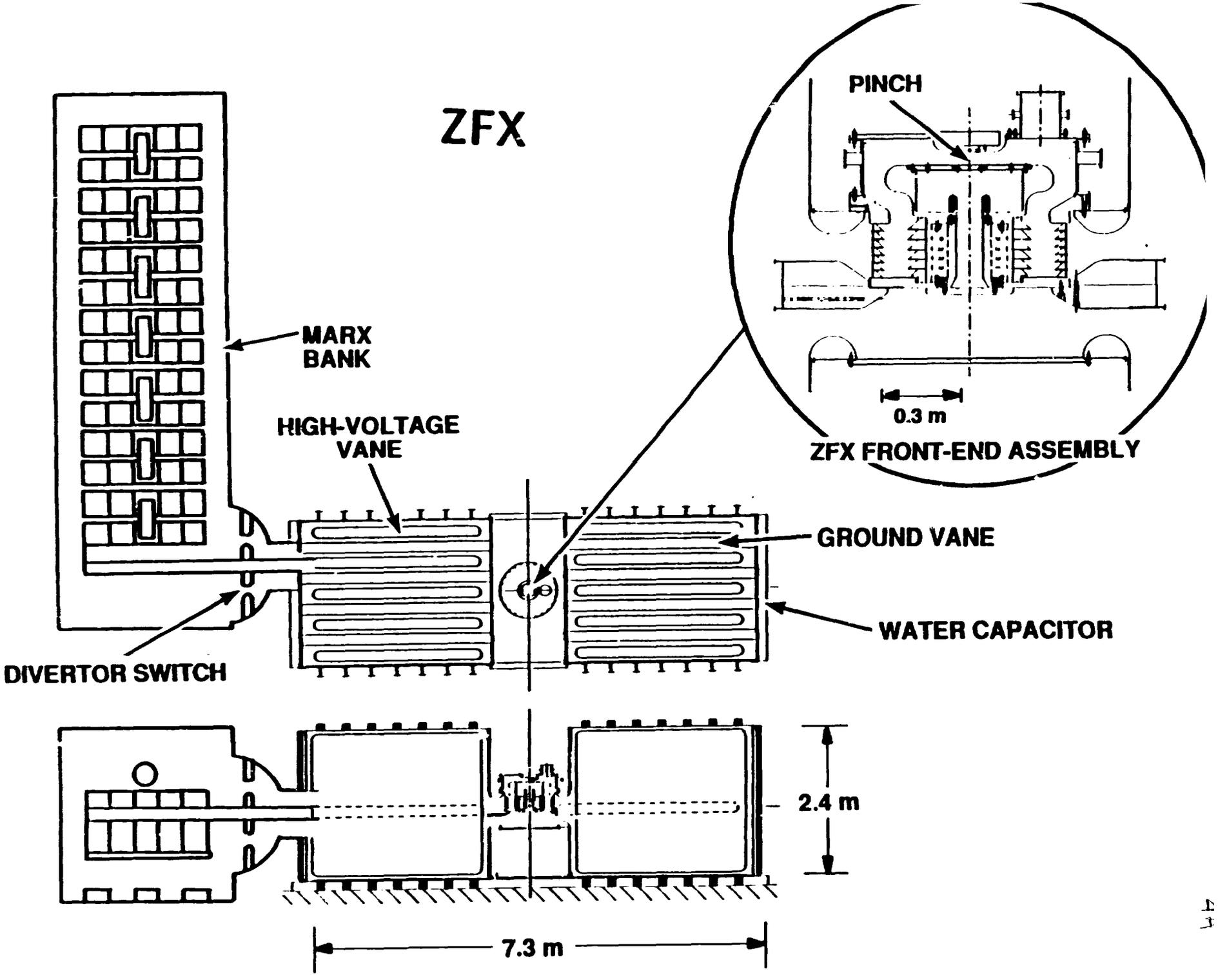
ZFX
PINCH
0.3 m
ZFX FRONT-END ASSEMBLY
MARX BANK
HIGH-VOLTAGE VANE
GROUND VANE
WATER CAPACITOR
DIVERTOR SWITCH
2.4 m
7.3 m

HDZP-II

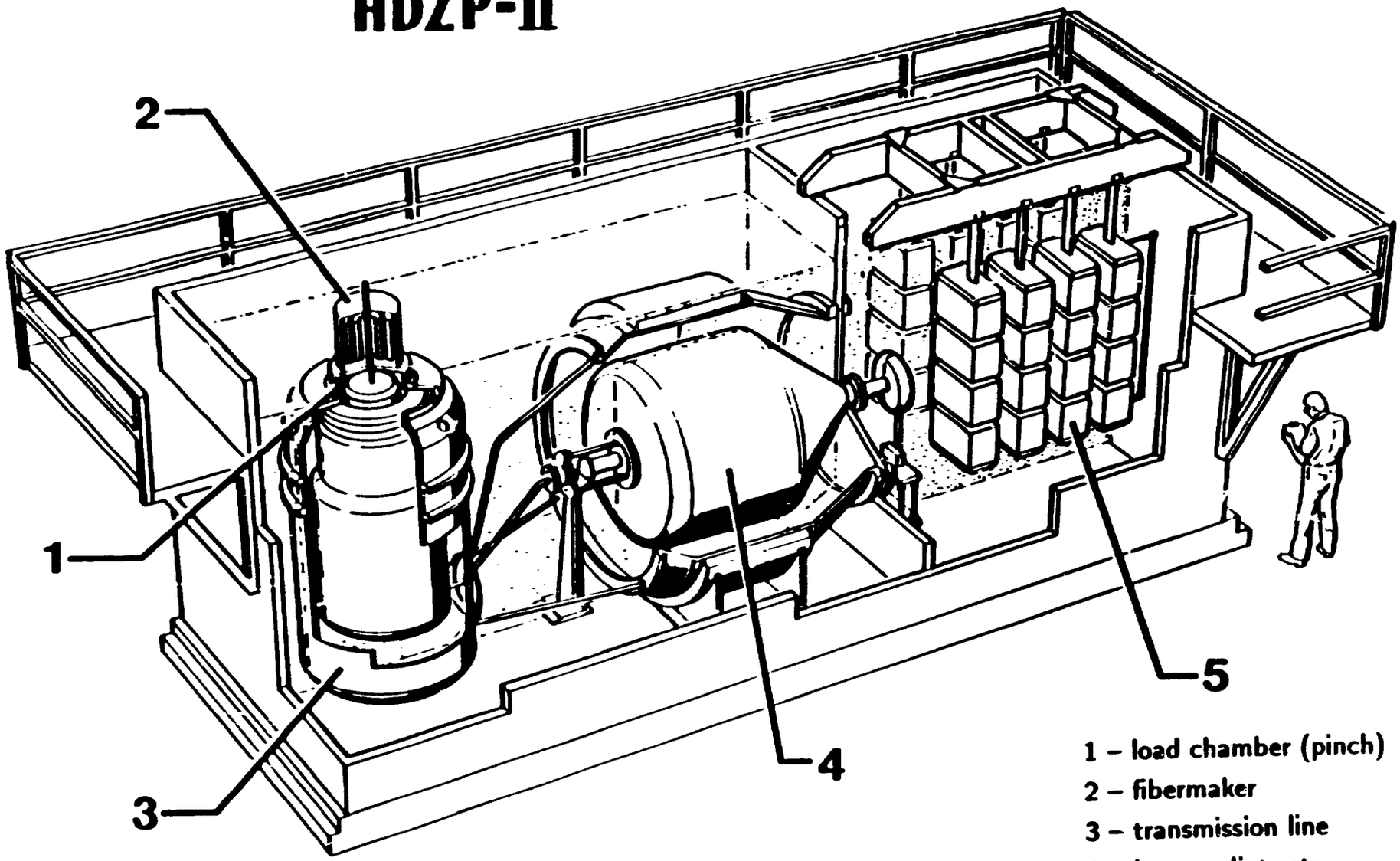

1 – load chamber (pinch)
2 – fibermaker
3 – transmission line
4 – intermediate store
5 – Marx bank

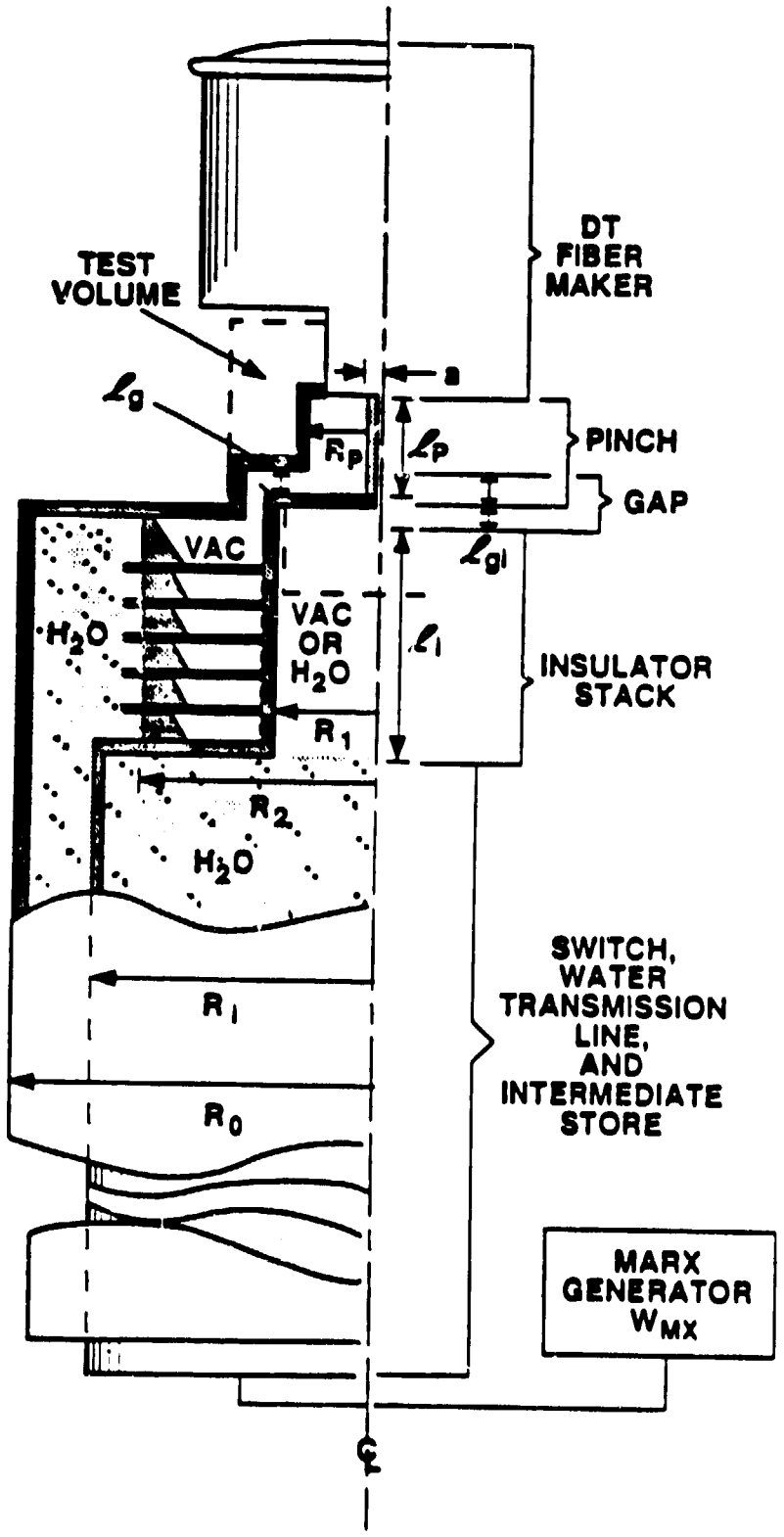
DT
FIBER
MAKER
TEST
VOLUME
a
ℓ_g
R_p
ℓ_p
PINCH
GAP
ℓ_{gl}
VAC
VAC
OR
H_2O
H_2O
ℓ_1
INSULATOR
STACK
R_1
R_2
H_2O
SWITCH,
WATER
TRANSMISSION
LINE,
AND
INTERMEDIATE
STORE
R_1
R_0
MARX
GENERATOR
W_{MX}
$\mathcal{L}$

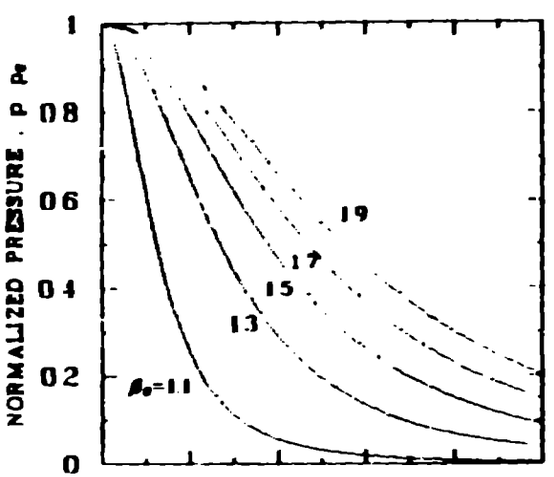
NORMALIZED PRESSURE , p/p0
1
0.8
0.6
0.4
0.2
0
β0=1.1
1.3
1.5
1.7
1.9

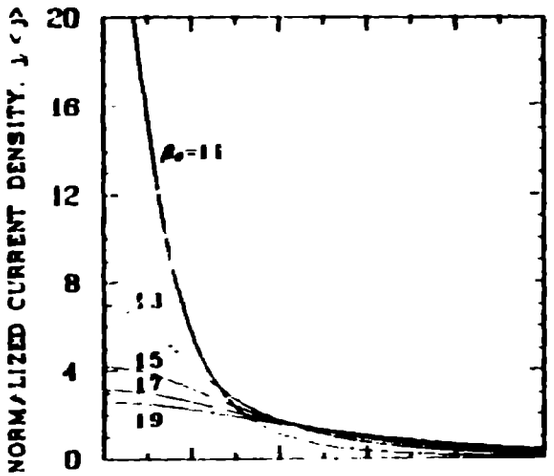
NORMALIZED CURRENT DENSITY, j/<j>
20
16
12
8
4
0
β0=1.1
1.3
1.5
1.7
1.9

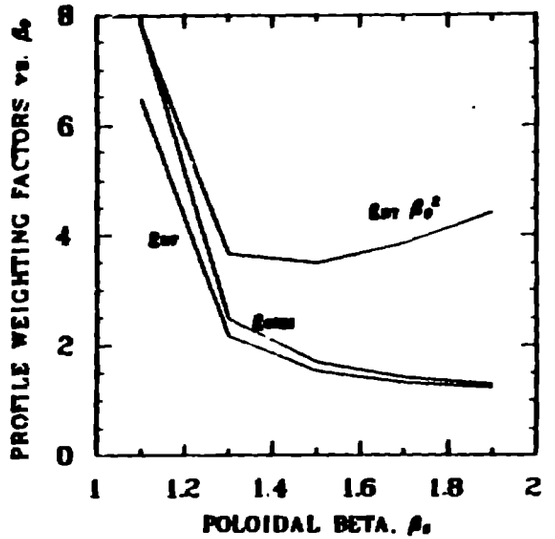
PROFILE WEIGHTING FACTORS vs. β0
8
6
4
2
0
1
1.2
1.4
1.6
1.8
2
POLOIDAL BETA, β0

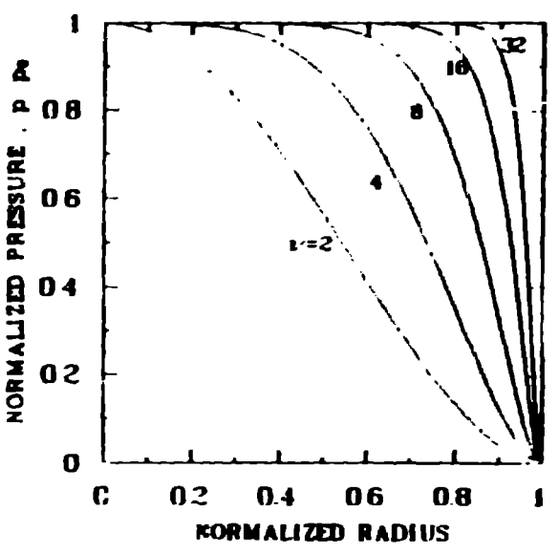
NORMALIZED PRESSURE , p/p0
1
0.8
0.6
0.4
0.2
0
0
0.2
0.4
0.6
0.8
1
NORMALIZED RADIUS
ν=2
4
8
16
32

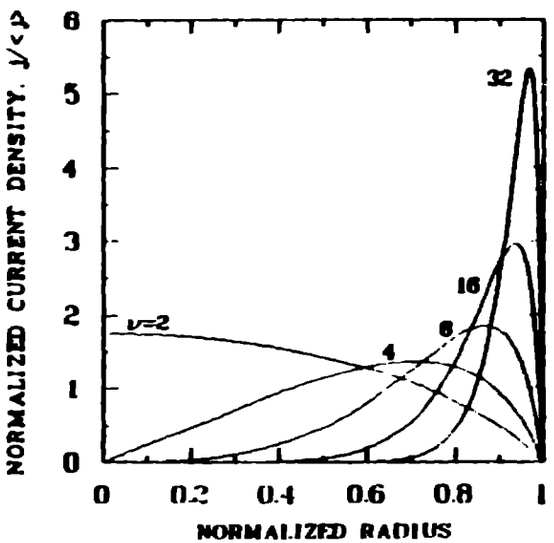
NORMALIZED CURRENT DENSITY, j/<j>
6
5
4
3
2
1
0
0
0.2
0.4
0.6
0.8
1
NORMALIZED RADIUS
ν=2
4
8
16
32

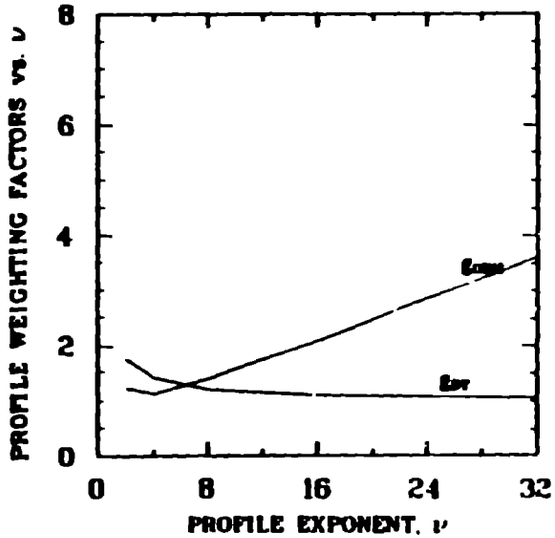
PROFILE WEIGHTING FACTORS vs. ν
8
6
4
2
0
0
8
16
24
32
PROFILE EXPONENT, ν

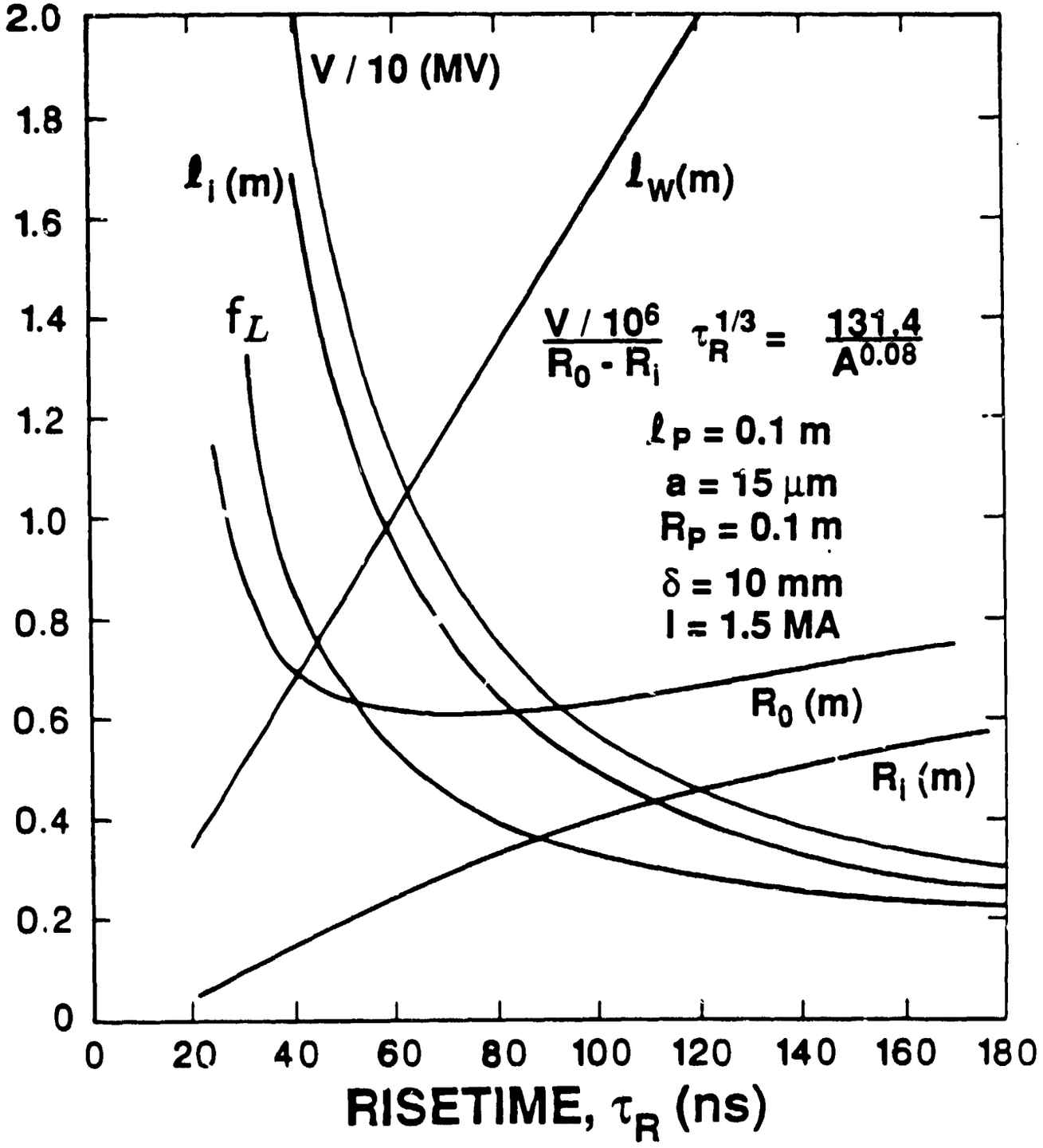
2.0
1.8
1.6
1.4
1.2
1.0
0.8
0.6
0.4
0.2
0
V / 10 (MV)
ℓ_i (m)
ℓ_W(m)
f_L
$\frac{V / 10^6}{R_0 - R_i} \tau_R^{1/3} = \frac{131.4}{A^{0.08}}$
ℓ_P = 0.1 m
a = 15 μm
R_P = 0.1 m
δ = 10 mm
I = 1.5 MA
R_0 (m)
R_i (m)
0
20
40
60
80
100
120
140
160
180
RISETIME, τ_R (ns)

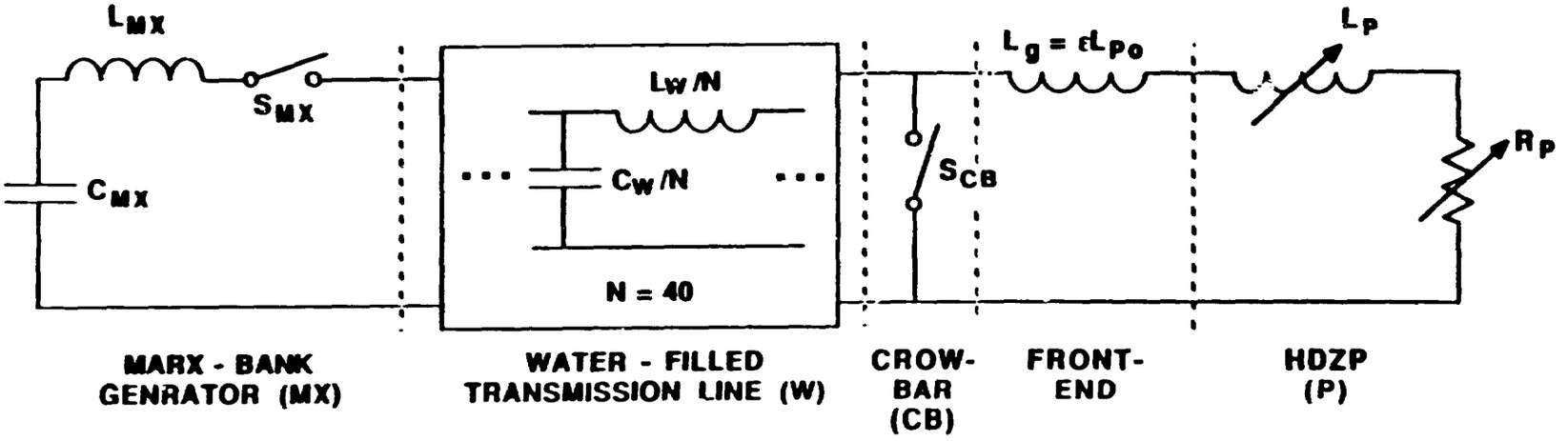
L_{MX}
S_{MX}
C_{MX}
L_W/N
C_W/N
N = 40
S_{CB}
$L_g = \epsilon L_{Po}$
L_P
R_P
MARX - BANK GENRATOR (MX)
WATER - FILLED TRANSMISSION LINE (W)
CROW-BAR (CB)
FRONT-END
HDZP (P)

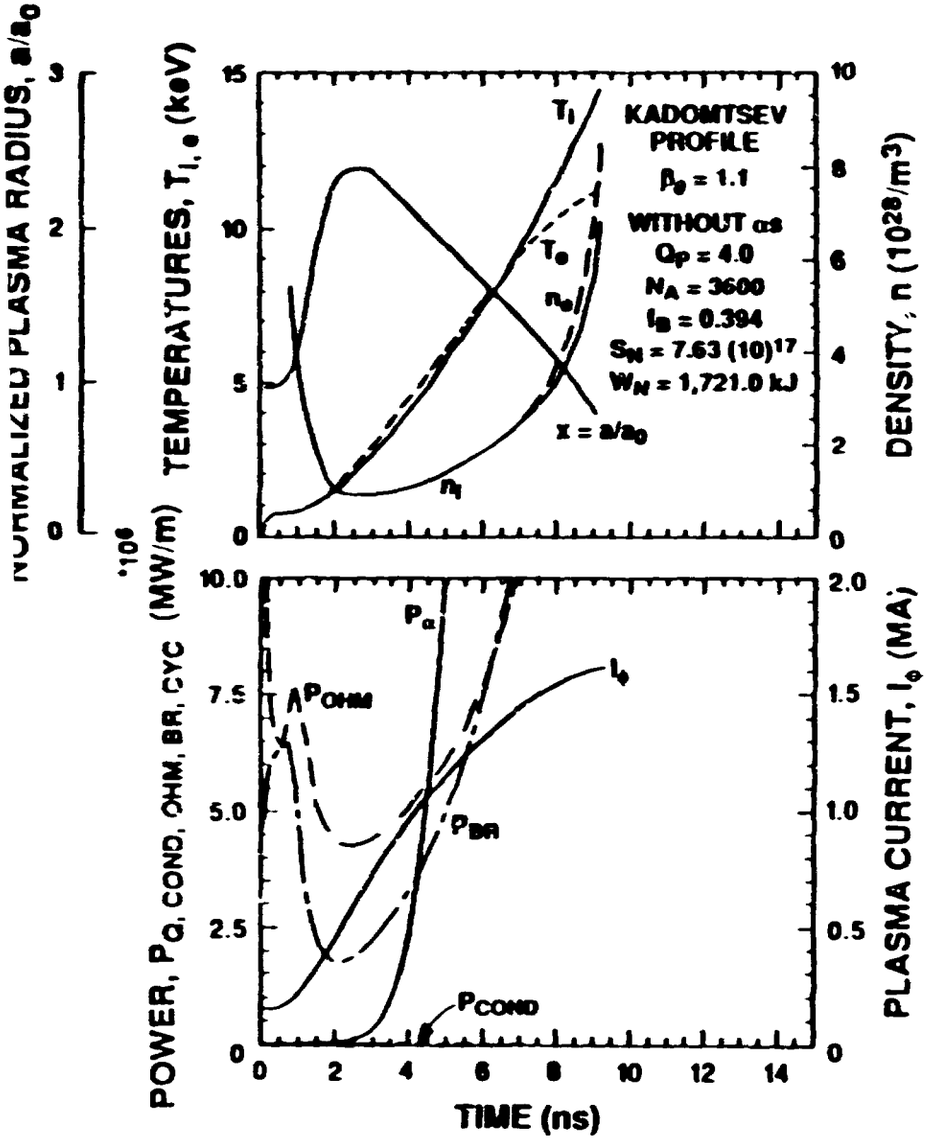
NORMALIZED PLASMA RADIUS, a/a0
TEMPERATURES, Ti, e (keV)
DENSITY, n (10^28/m^3)
KADOMTSEV PROFILE
β0 = 1.1
WITHOUT αs
Qp = 4.0
NA = 3600
fB = 0.394
SN = 7.63 (10)^17
WN = 1,721.0 kJ
Ti
Te
ne
ni
x = a/a0
POWER, Pα, COND, OHM, BR, CYC (MW/m)
PLASMA CURRENT, Iφ (MA)
Pα
POHM
PBR
PCOND
Iφ
TIME (ns)

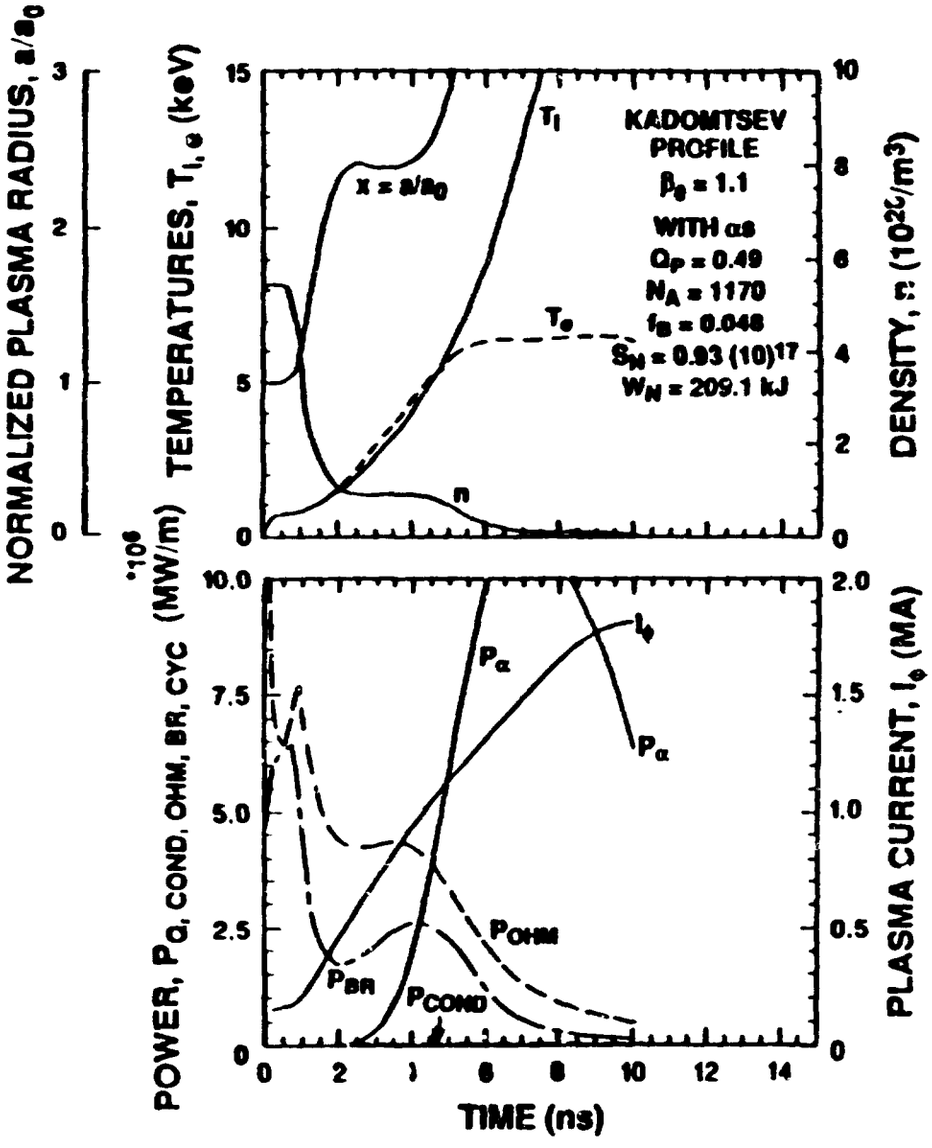
NORMALIZED PLASMA RADIUS, a/a0
TEMPERATURES, Ti, e (keV)
DENSITY, n (10^28/m^3)
KADOMTSEV PROFILE
β0 = 1.1
WITH αs
Qp = 0.49
NA = 1170
fB = 0.048
SN = 0.93 (10)^17
WN = 209.1 kJ
Ti
Te
n
x = a/a0
POWER, Pα, COND, OHM, BR, CYC (MW/m)
PLASMA CURRENT, Iφ (MA)
Pα
POHM
PBR
PCOND
Iφ
TIME (ns)

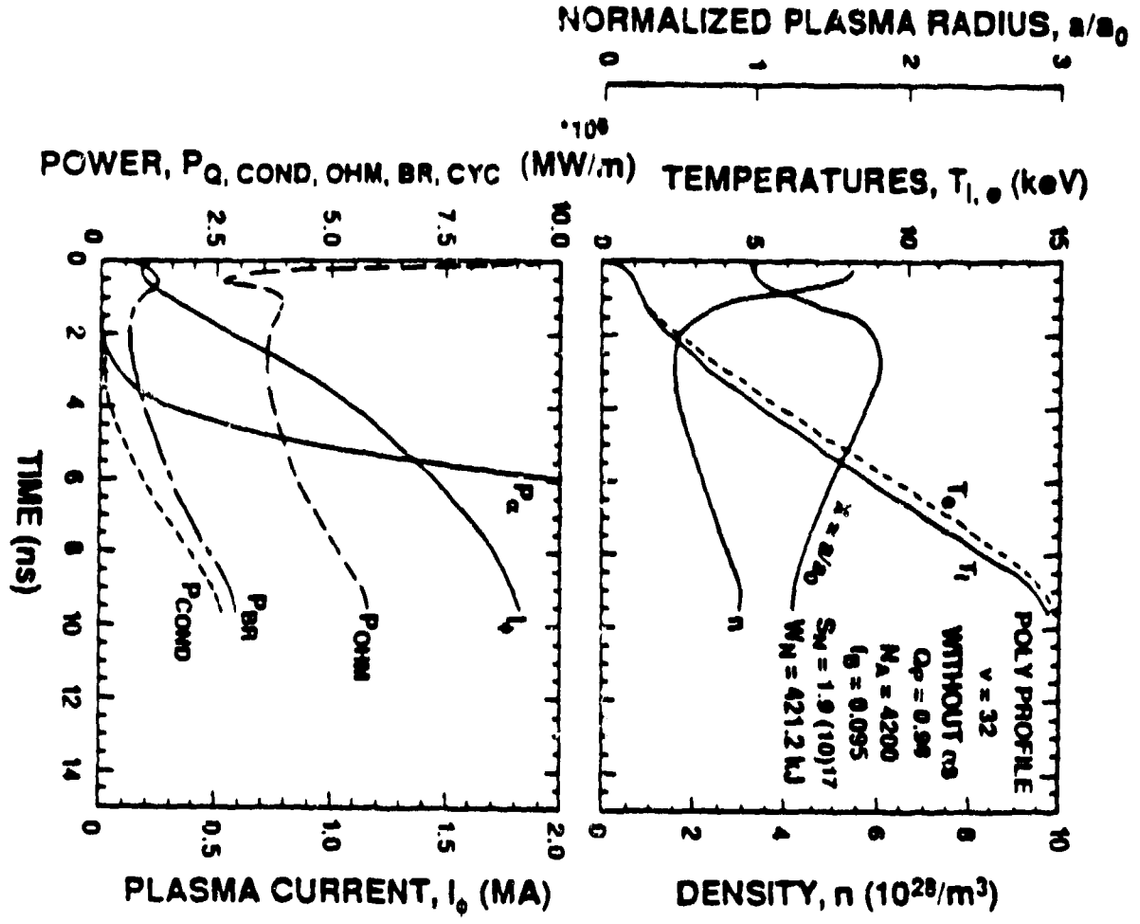
NORMALIZED PLASMA RADIUS, a/a0
POWER, PQ, COND, OHM, BR, CYC (MW/m)
TEMPERATURES, Ti, e (keV)
TIME (ns)
PCOND
PBR
POHM
Pα
Iϕ
Te
Ti
n
x = a/a0
POLY PROFILE
ν = 32
WITHOUT ωs
Qp = 0.96
NA = 4200
Iϕ = 0.095
SN = 1.9 (10)17
WN = 421.2 kJ
PLASMA CURRENT, Iϕ (MA)
DENSITY, n (10^28/m^3)

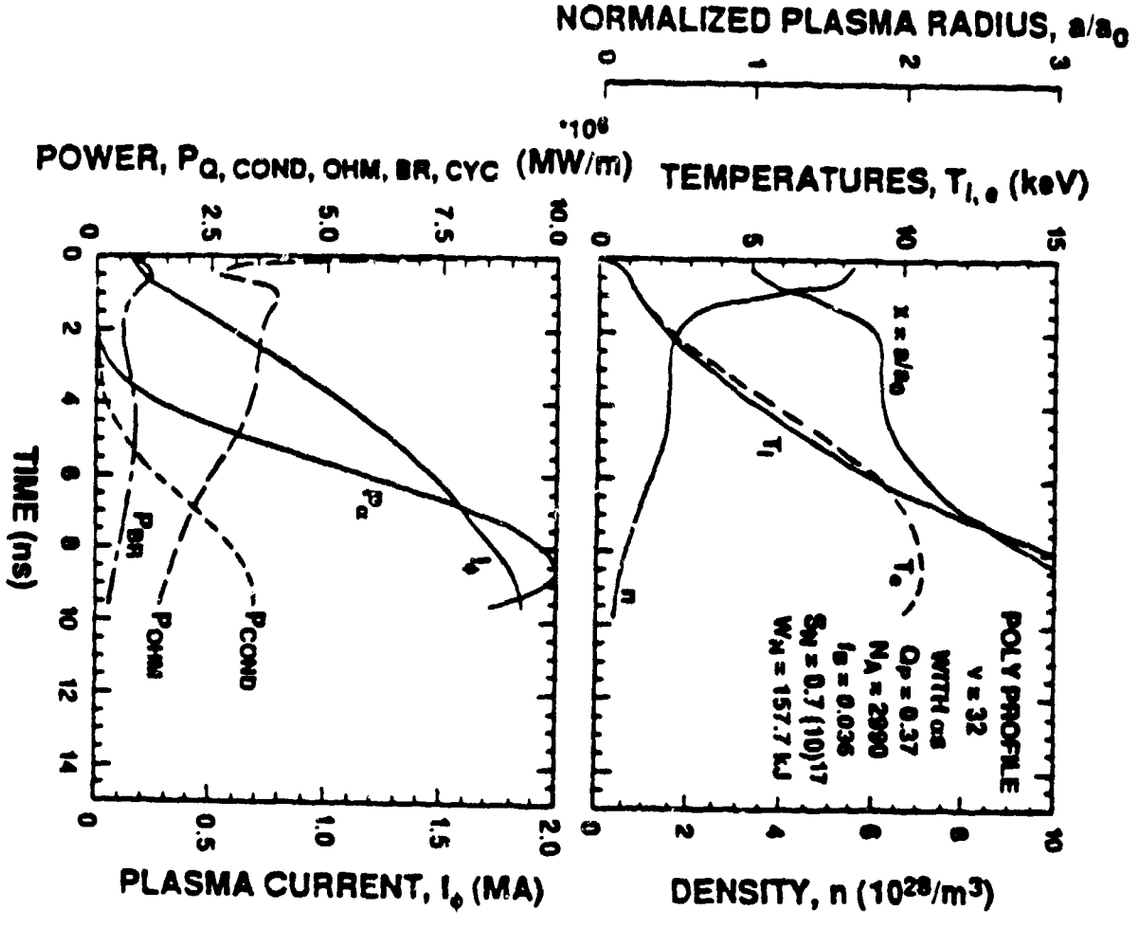
NORMALIZED PLASMA RADIUS, a/a0
POWER, PQ, COND, OHM, BR, CYC (MW/m)
TEMPERATURES, Ti, e (keV)
TIME (ns)
PCOND
PBR
POHM
Pα
Iϕ
Te
Ti
n
x = a/a0
POLY PROFILE
ν = 32
WITH ωs
Qp = 0.37
NA = 2900
Iϕ = 0.036
SN = 0.7 (10)17
WN = 157.7 kJ
PLASMA CURRENT, Iϕ (MA)
DENSITY, n (10^28/m^3)

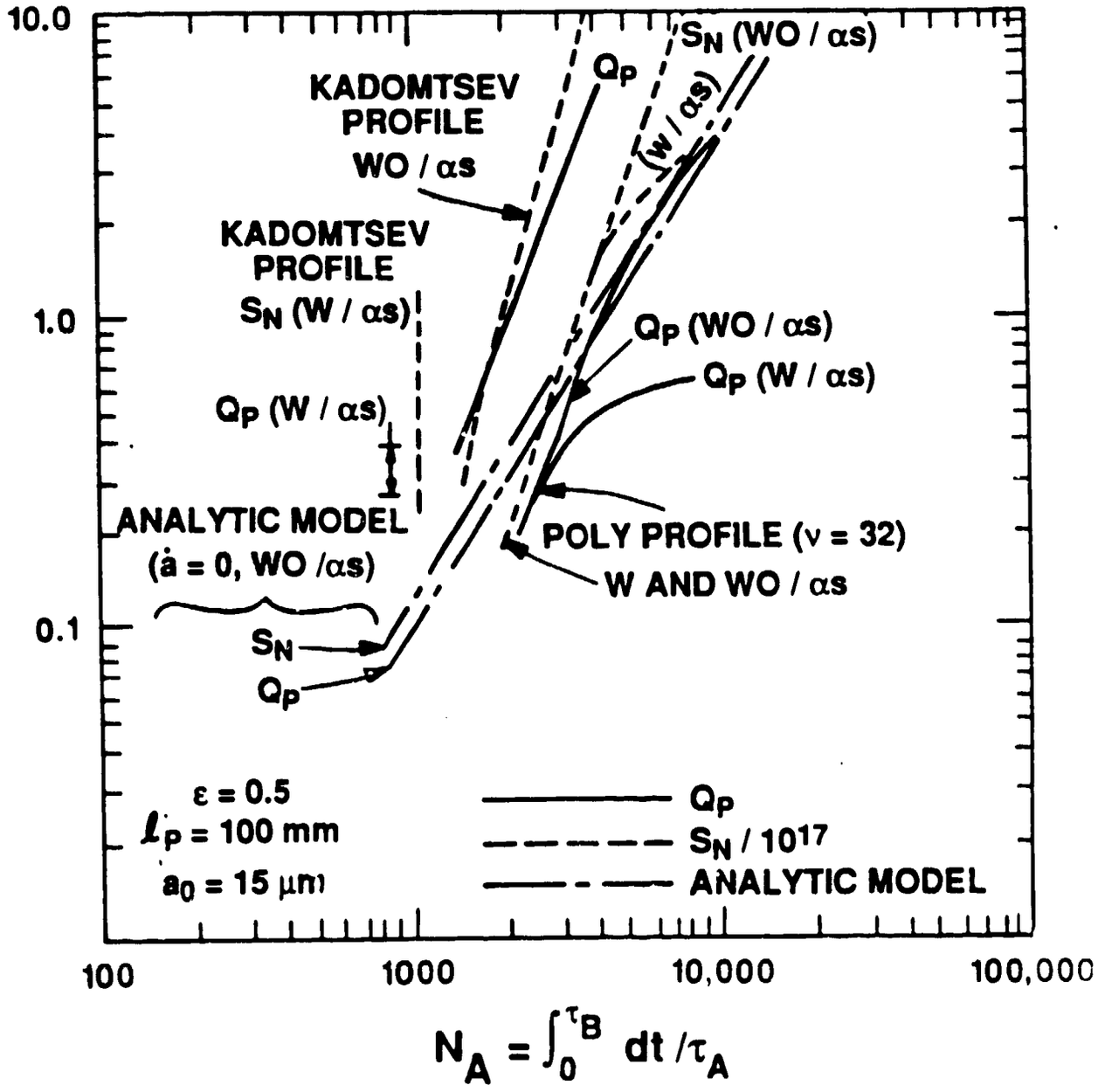
10.0
1.0
0.1
100
1000
10,000
100,000
KADOMTSEV PROFILE
WO / αs
KADOMTSEV PROFILE
SN (W / αs)
QP (W / αs)
ANALYTIC MODEL
(ȧ = 0, WO /αs)
SN
QP
SN (WO / αs)
QP
(W / αs)
QP (WO / αs)
QP (W / αs)
POLY PROFILE (ν = 32)
W AND WO / αs
ε = 0.5
ℓP = 100 mm
a0 = 15 μm
QP
SN / 10^17
ANALYTIC MODEL
$N_A = \int_0^{\tau_B} dt / \tau_A$

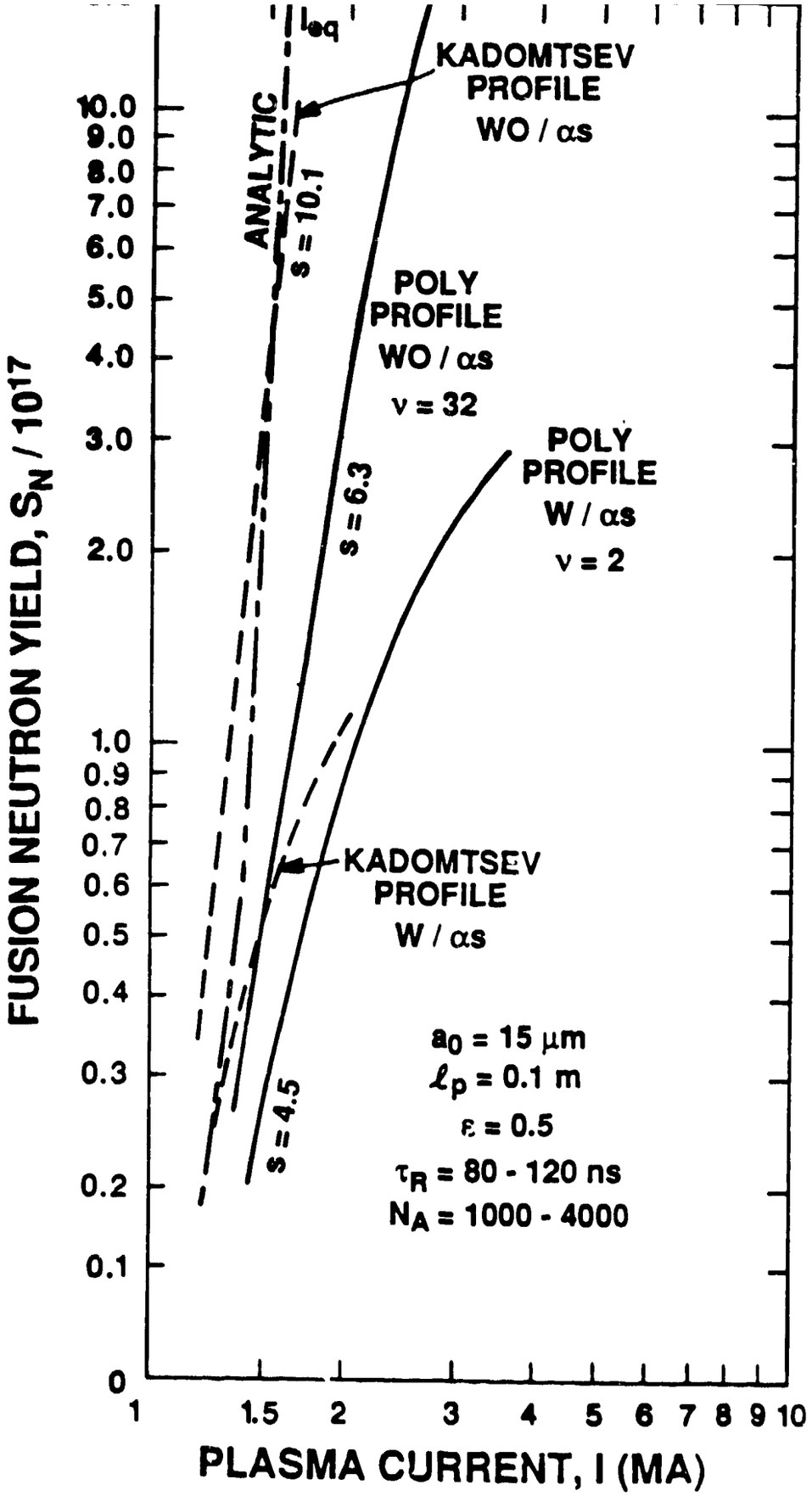
FUSION NEUTRON YIELD, S_N / 10^{17}
PLASMA CURRENT, I (MA)
I_{eq}
ANALYTIC
s = 10.1
KADOMTSEV PROFILE WO / αs
POLY PROFILE WO / αs ν = 32
s = 6.3
POLY PROFILE W / αs ν = 2
KADOMTSEV PROFILE W / αs
s = 4.5
a_0 = 15 μm
ℓ_p = 0.1 m
ε = 0.5
τ_R = 80 - 120 ns
N_A = 1000 - 4000
10.0
9.0
8.0
7.0
6.0
5.0
4.0
3.0
2.0
1.0
0.9
0.8
0.7
0.6
0.5
0.4
0.3
0.2
0.1
0
1
1.5
2
3
4
5
6
7
8
9
10

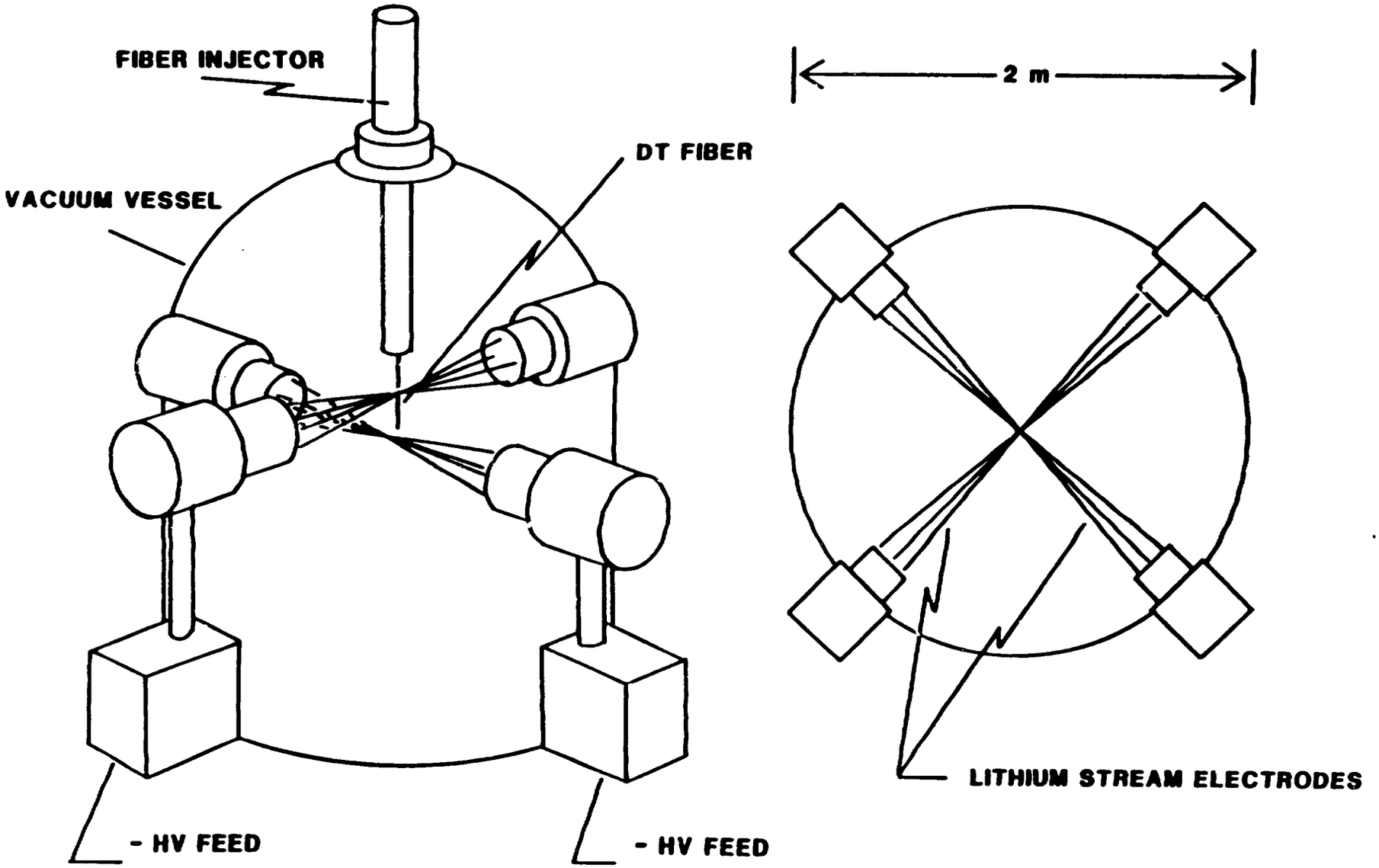
FIBER INJECTOR
DT FIBER
VACUUM VESSEL
- HV FEED
- HV FEED
2 m
LITHIUM STREAM ELECTRODES

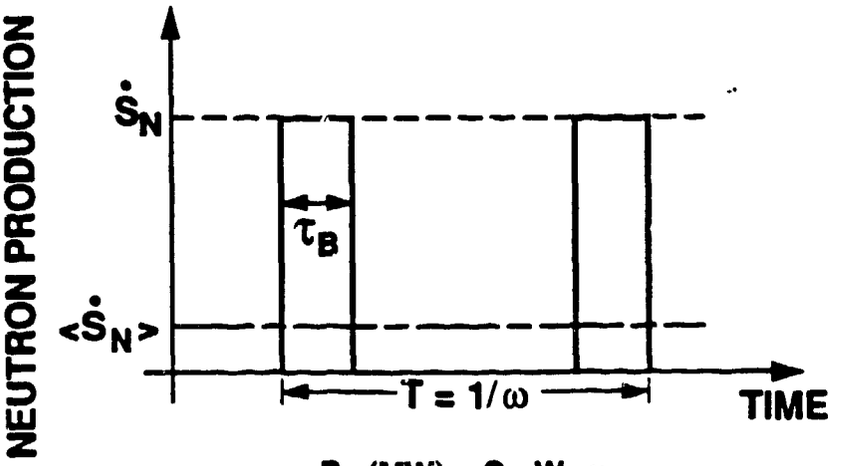

$$P_F\ (MW) = Q_p\ W_B\ \omega$$

$$= 28\ \frac{\langle \dot{S}_N \rangle}{10^{19}}$$

$$\frac{2\langle \dot{S}_N \rangle}{N \mathcal{L}_p} = f_B \omega$$

$$\langle \dot{S}_N \rangle = \dot{S}_N\ \tau_B\ \omega$$

$$\text{FLUX COMPRESSION} = FC = \dot{S}_N / \langle \dot{S}_N \rangle = \frac{1}{\tau_B\ \omega}$$

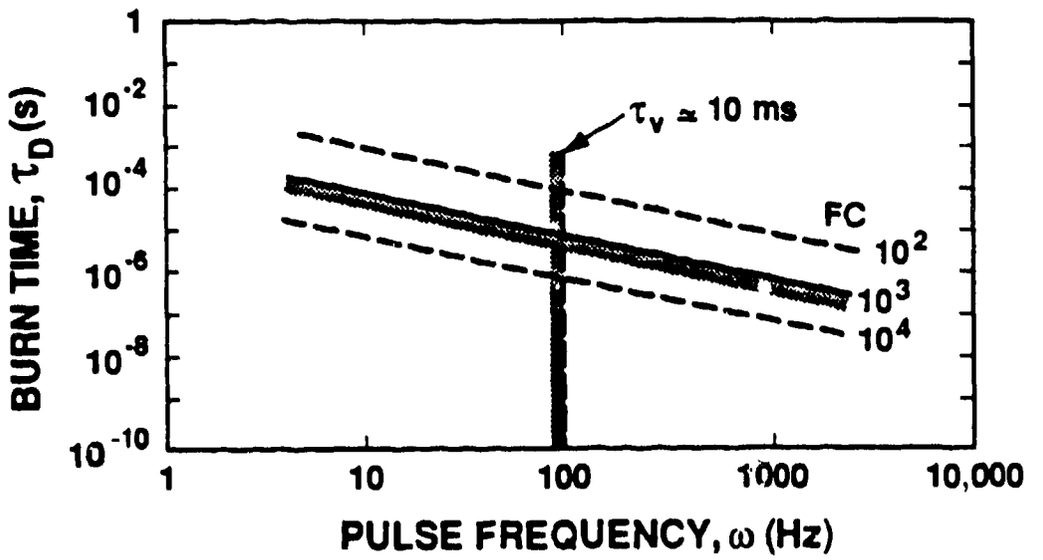

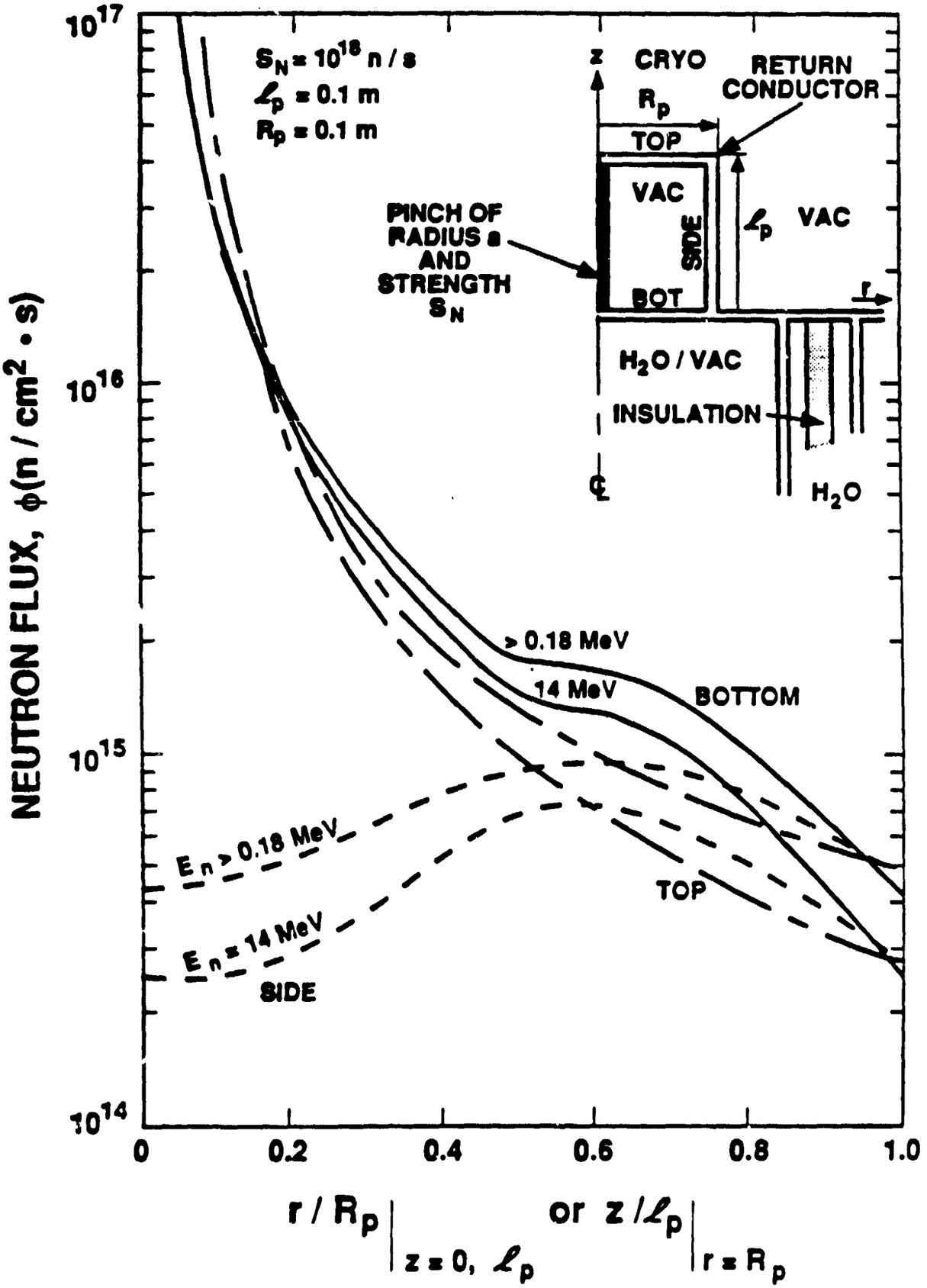
$S_N = 10^{18}$ n / s
ℓ_p = 0.1 m
R_p = 0.1 m
z
CRYO
RETURN CONDUCTOR
R_p
TOP
VAC
SIDE
ℓ_p
VAC
BOT
r
PINCH OF RADIUS a AND STRENGTH S_N
H_2O / VAC
INSULATION
H_2O
> 0.18 MeV
14 MeV
BOTTOM
TOP
E_n > 0.18 MeV
E_n = 14 MeV
SIDE
NEUTRON FLUX, ϕ(n / cm^2 • s)
10^{17}
10^{16}
10^{15}
10^{14}
0
0.2
0.4
0.6
0.8
1.0
$r / R_p \Big|_{z = 0,\ \ell_p}$ or $z / \ell_p \Big|_{r = R_p}$

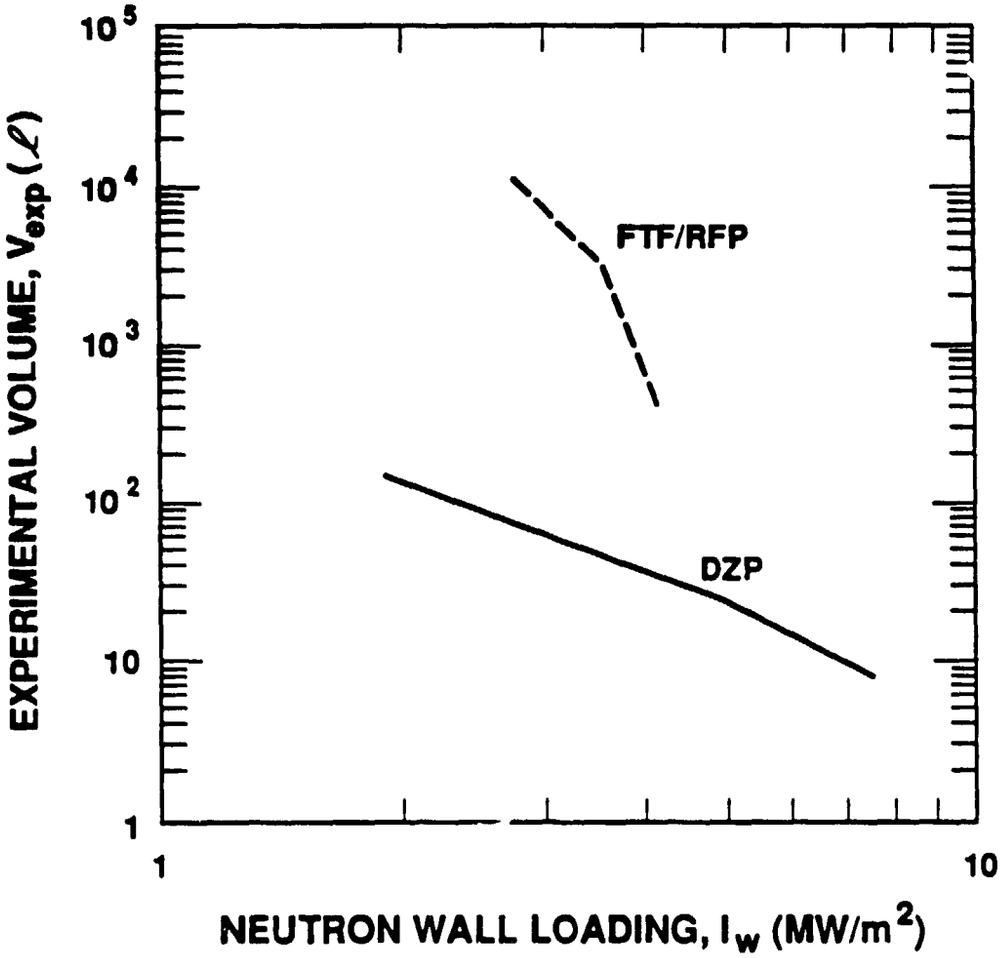
EXPERIMENTAL VOLUME, V_{exp} (ℓ)
10^5
10^4
10^3
10^2
10
1
FTF/RFP
DZP
1
10
NEUTRON WALL LOADING, I_w (MW/m^2)

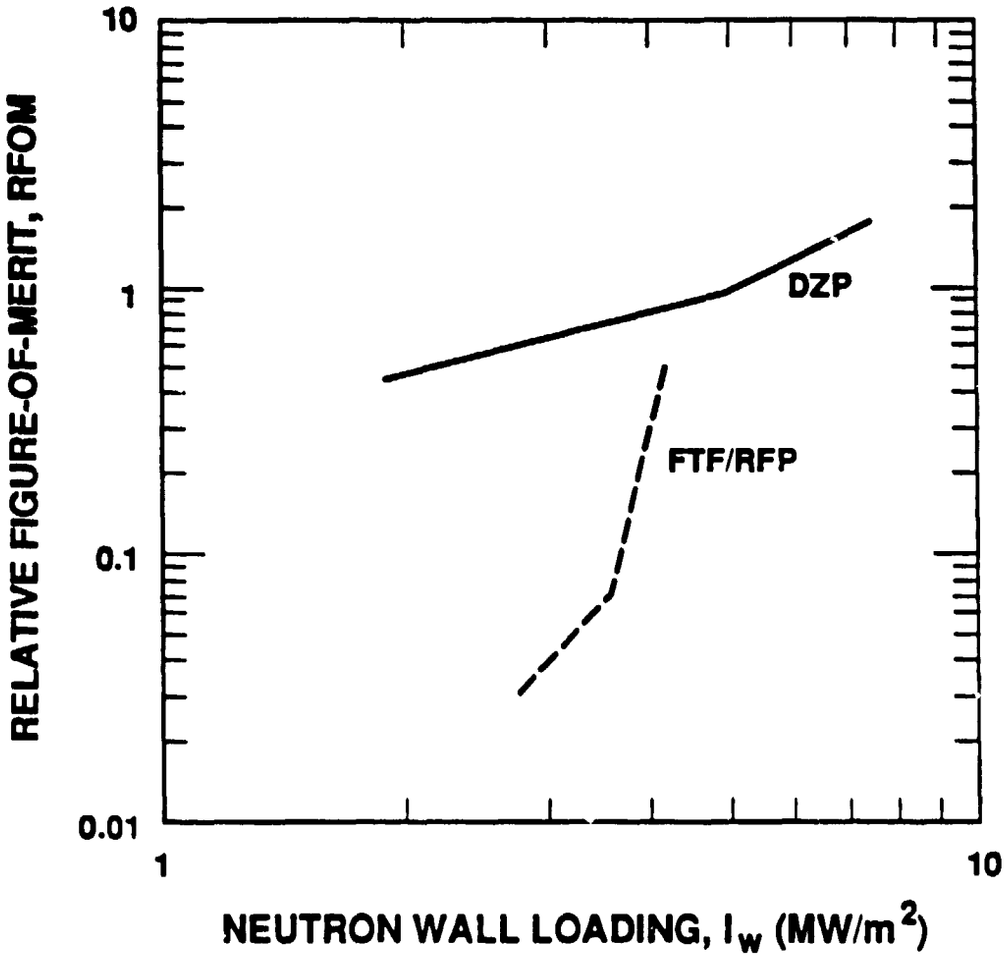
10
1
0.1
0.01
1
10
RELATIVE FIGURE-OF-MERIT, RFOM
NEUTRON WALL LOADING, I_w (MW/m^2)
DZP
FTF/RFP